

## V. THEORETICAL PHYSICS

### OVERVIEW

Our research addresses important problems in theoretical nuclear astrophysics and nuclear physics involving the structure and dynamics of hadrons and nuclei. There is strong emphasis on comparison with data from Argonne's ATLAS facility, from JLab, and from other laboratories around the world, and identifying and predicting phenomena that can be explored with a rare isotope accelerator. Our work includes the modeling and application of quantum chromodynamics (QCD) to light- and heavy-hadron structure at zero temperature and density, and at the extremes of temperature and density appropriate to the early universe, neutron stars, and RHIC experiments. We develop reaction theories to use in exploring hadron structure using the data from meson and nucleon-resonance production experiments at JLab, MIT-Bates and Mainz. We construct realistic two- and three-nucleon potentials that give accurate fits to nucleon-nucleon elastic scattering data and properties of light nuclei, and use them in detailed many-body calculations of light and near closed-shell nuclei, nuclear matter and neutron stars, and in a variety of astrophysically important electroweak reactions. We investigate nuclear processes that take place in stars, in the big bang, and in interstellar and intergalactic space. Our nuclear structure and reaction studies include coupled-channels calculations of heavy-ion reactions near the Coulomb barrier, and calculations of observables in breakup reactions of nuclei far from stability. We also study high-spin deformation and the structure of the heaviest elements at the mean-field level, and work toward an understanding of the interplay between collective modes at the many-body level. Additional research is pursued in atomic physics, neutron physics, quantum computing, and fundamental quantum mechanics. Several of our projects involve major numerical simulations using the massively parallel computer systems at Argonne and NERSC. Many projects also involve collaborators, students and staff, at US and foreign universities, and other national laboratories.

## A. NUCLEAR DYNAMICS WITH SUBNUCLEONIC DEGREES OF FREEDOM

The objective of this research program is to investigate the role of: quark-gluon degrees of freedom in hadron structure and interactions, and in nuclear dynamics; the development and application of reaction theories for use in exploring hadron structure using the data from meson and nucleon-resonance production experiments at modern experimental facilities; and to investigate relations of Poincaré covariant dynamics specified by mass operators to complementary dynamics specified by Green functions.

At the level of quark-gluon degrees of freedom, the Dyson-Schwinger equations (DSEs) provide a Poincaré covariant, nonperturbative method for studying QCD in the continuum. The existence of symmetry preserving truncations enables the simultaneous exploration of phenomena such as: confinement, dynamical chiral symmetry breaking, and bound state structure and interactions, and means that model studies facilitate the use of physical processes to constrain the long-range behavior of the quark-quark interaction. In this last year we established a direct connection between a standard lattice-QCD expression for the vacuum quark condensate and those valid in the continuum, and a practical means of comparing the calculated results. We showed, too, that quenched lattice-QCD data on the dressed-quark and -gluon propagators can be correlated via a rainbow gap equation so long as that equation's kernel possesses enhancement at infrared momenta. This analysis also suggests that many physical quantities are materially underestimated in quenched lattice-QCD. In addition, we began the study of meson excited states and established the exact result that in theories which exhibit dynamical chiral symmetry breaking the leptonic decay constant of every pseudoscalar meson, except the ground state, vanishes in the chiral limit. Thus, in chiral-QCD,  $f_{\pi(140)} \neq 0$  but this decay constant vanishes for every one of the pion's radial excitations. Furthermore, using a quark-diquark model of the nucleon, we illustrated that, on the domain of  $q^2$  accessible in modern precision experiments, the proton's elastic electromagnetic form factors are a sensitive probe of nonperturbative strong interaction dynamics.

At the level of meson and baryon degrees of freedom, we focus our effort on developing dynamical models for investigating few-GeV electromagnetic meson production reactions. Our objective is an interpretation of the very extensive data from JLab in terms of the quark-gluon substructure of nucleon resonances ( $N^*$ ) as predicted by various QCD-based hadron models and simulations of lattice-QCD. In the past year we succeeded in extending our dynamical model for the  $\Delta$  excitation, to include additional meson-baryon channels ( $\eta N$ ,  $\omega N$ ,  $KY$ ) and the three-body  $\pi\pi N$  channels ( $\pi\Delta$ ,  $\rho N$ ). The resulting multi-channel, multi-resonance model was used to expose the effect of a meson cloud on the resonance parameters of  $N^*(1535)$  and  $N^*(1650)$ . It was also applied to analyze the reaction mechanisms for low energy  $\rho$ -meson photoproduction and kaon-hyperon reactions, and we attempted to interpret the bare  $\gamma N \rightarrow \Delta$  transition form factor, which was inferred from pion electroproduction data using our model, in terms of a light-front constituent-quark model. We also explored the production mechanisms of the recently observed, narrow-width  $\Theta^+$  resonance and found that double polarization observables in the  $\vec{\gamma} \vec{n} \rightarrow K^+ K^- n$  reaction are sensitive to the parity of the  $\Theta^+$ . Hence a realistic  ${}^3\overline{He}(\vec{\gamma}, K^+ K^- n)$  experiment can decisively determine whether  $\Theta^+$  is truly a pentaquark state. A new project was initiated to investigate medium effects on  $\rho$  propagation in nuclei, which aims at examining whether the

current interpretation of dilepton production from relativistic heavy-ion collisions in terms of medium effects is valid.

Relativistic quantum dynamics requires a unitary representation of space-time symmetries (Poincaré group) and localization of states, such that states localized in relatively space-like regions are causally independent. Recent mathematical developments indicate how manifolds of localized states can be defined strictly within the framework of relativistic quantum mechanics without reference to infinite systems.

### a.1. Dyson-Schwinger Equations and Hadron Physics (C. D. Roberts and P. Maris\*)

Dyson-Schwinger equations (DSEs) furnish a Poincaré covariant framework within which to study hadrons. However, their application has long been plagued by concerns over the need to employ a truncation scheme in order to arrive at a tractable problem. It was recently shown that there exists at least one systematic, nonperturbative, symmetry-preserving DSE truncation procedure; and this has enabled the proof of exact, model-independent results. For example, the gap equation reveals that dynamical chiral symmetry breaking is tied to the long-range behavior of the strong interaction, which is thereby constrained by observables, and the pion is precisely understood, and seen to exist simultaneously as a Goldstone mode and a bound state of strongly dressed quarks. The rainbow-ladder truncation is the leading-order term in the

systematic scheme. That realization has enabled the systematic error associated with this simplest truncation to be quantified, and that explains and underpins a one-parameter model efficacious in describing an extensive body of mesonic phenomena. Incipient applications to baryons have brought successes and encountered challenges familiar from early studies of mesons, and promise a covariant field theory upon which to base an understanding of contemporary large momentum transfer data. This body of work reveals that the momentum-dependent *dressing* of the propagators of QCD's elementary excitations is a fundamental feature of strong QCD that is observable in hadron physics. We published an extensive review<sup>1</sup> explaining these foundations and reviewing many applications.

\*North Carolina State University.

<sup>1</sup>P. Maris and C. D. Roberts, Int. J. Mod. Phys. **E12**, 297-365 (2003).

### a.2. Facets of Confinement and Dynamical Chiral Symmetry Breaking (P. Maris,\* A. Raya,† C. D. Roberts, and S. M. Schmidt‡)

The gap equation is a cornerstone in understanding dynamical chiral symmetry breaking and, perhaps, confinement too. The existence of a symmetry-preserving truncation enables proofs of important results and also a gap-equation-based analysis of contemporary lattice data on quark and gluon propagators. The available lattice data is for quenched

QCD and this exploratory study suggests that physical observables are materially underestimated in the quenched theory: the pion decay constant by as much as a factor of two. In addition it re-emphasizes that multiplicative renormalizability can provide very useful constraints on the gap equation's kernel. An article describing this research was published.<sup>1</sup>

\*North Carolina State University, †Universidad Michoacana de San Nicolás de Hidalgo, Mexico, ‡Helmholtz-Gemeinschaft, Germany.

<sup>1</sup>P. Maris, A. Raya, C. D. Roberts, and S. M. Schmidt, Eur. Phys. J. **A18**, 231-235 (2003).

### a.3. Concerning the Quark Condensate (C. D. Roberts, K. Langfeld,\* R. Pullirsch,† H. Markum,† and S. M. Schmidt‡)

We verified that the gauge-invariant trace of the massive dressed-quark propagator possesses a spectral representation, with a non-negative spectral density  $\rho(\lambda)$ , when considered as a function of the current-quark mass. This is key to establishing that the OPE condensate, which sets the ultraviolet scale for the momentum-

dependence of the trace of the dressed-quark propagator, does indeed measure the density of far-infrared eigenvalues of the gauge-averaged massless Dirac operator, à la the Banks-Casher relation. This relation is intuitively appealing because a measurable accumulation of eigenvalues of the massless Dirac operator

\*University of Tübingen, Germany, †Technical University of Vienna, Austria, ‡Helmholtz-Gemeinschaft, Germany.

<sup>1</sup>K. Langfeld, R. Pullirsch, H. Markum, C. D. Roberts, and S. M. Schmidt, Phys. Rev. C **67**, 065206 (2003).

at zero-virtuality expresses a mass gap in its spectrum. In our continuum analysis we found that one requires  $am \leq (a\Lambda_{\text{QCD}})^3$  if  $\rho(\lambda) = 0$  is to provide a veracious estimate of the OPE condensate. The residue at the

lowest-mass pole in the flavor-nonsinglet pseudoscalar vacuum polarization provides a measure of the OPE condensate that is accurate for larger current-quark masses. An article describing this work was published.<sup>1</sup>

#### a.4. Analysis of a Quenched Lattice-QCD Dressed-Quark Propagator

(C. D. Roberts, M. S. Bhagwat,\* M. A. Pichowsky,\* and P. C. Tandy\*)

We studied quenched-QCD using a rainbow-ladder truncation of the Dyson-Schwinger equations and demonstrated that existing results from lattice simulations for the dressed-gluon and quark Schwinger functions can be correlated via a gap equation. As usual, the ultraviolet behavior of this equation's effective interaction is fully determined by perturbative QCD. For the infrared, we employed a simple *Ansatz* whose parameters were fixed in a least squares fit of the gap equation's solutions to lattice data on the dressed-quark mass function at available current-quark masses. With our best-fit parameters the mass functions obtained from the gap equation were indistinguishable from the lattice results. To correlate the lattice's dressed-gluon and dressed-quark Schwinger functions it was necessary for the kernel to exhibit

infrared enhancement over and above that observed in the dressed-gluon function alone. In our model we ascribed that to an enhancement of the quark-gluon vertex. The gap equation provides a solution for the dressed-quark Schwinger function at arbitrarily small current-quark masses and, in particular, in the chiral limit: no extrapolation is involved. It may therefore be used as a tool with which to estimate the chiral limit behavior of the lattice propagator. In addition, knowing the gap equation's kernel, it is straightforward to construct symmetry-preserving Bethe-Salpeter equations whose bound state solutions describe mesons. This enabled an analysis which indicates that chiral and physical pion observables are significantly smaller in the quenched theory than in full QCD. An article describing this work was published.<sup>1</sup>

---

\*Kent State University.

<sup>1</sup>M. S. Bhagwat, M. A. Pichowsky, C. D. Roberts, and P. C. Tandy, Phys. Rev. C **68**, 015203 (2003).

#### a.5. Aspects and Consequences of a Dressed-Quark-Gluon Vertex

(M. S. Bhagwat,\* A. Höll, A. Krassnigg, C. D. Roberts, and P. C. Tandy\*)

We explored features of the dressed-quark-gluon vertex and their role in the gap and Bethe-Salpeter equations. It became apparent that quenched lattice data indicate the existence of net attraction in the colour-octet projection of the quark-antiquark scattering kernel. We saw that this attraction affects the uniformity with which solutions of truncated equations converge pointwise to solutions of the complete gap and vertex equations. We observed that for current-quark masses less than the scale set by dynamical chiral symmetry breaking, the dependence of the dressed-quark-gluon vertex on the current-quark mass is weak. Our analysis employed a vertex model whose diagrammatic content is explicitly enumerable. That enabled the systematic construction of a vertex-consistent Bethe-Salpeter kernel and thereby an exploration of the consequences for the strong interaction spectrum of attraction in the

colour-octet channel. We found that with rising current-quark mass the rainbow-ladder truncation provides an increasingly accurate estimate of a bound state's mass. Moreover, the calculated splitting between vector and pseudoscalar meson masses vanishes as the current-quark mass increases, which argues for the mass of the pseudoscalar partner of the  $Y(1S)$  to be above 9.4 GeV. Our calculations showed that the absence of colour-antitriplet diquarks from the strong interaction spectrum is contingent upon the net amount of attraction in the octet projected quark-antiquark scattering kernel. While there is a window within which diquarks appear, the amount of attraction suggested by lattice results is outside this domain. An article describing this work was submitted for publication.

---

\*Kent State University.

### a.6. Regarding Proton Form Factors (J. C. R. Bloch,\* A. Krassnigg, and C. D. Roberts)

The proton's elastic electromagnetic form factors were calculated using an *Ansatz* for the nucleon's Poincaré covariant Faddeev amplitude that only retains scalar diquark correlations. A spectator approximation was employed for the current. On the domain of  $q^2$  accessible in modern precision experiments these form factors are a sensitive probe of nonperturbative strong interaction dynamics. We found that the ratio of Pauli and Dirac form factors can provide realistic constraints

on models of the nucleon and thereby assist in developing an understanding of nucleon structure. The ratio of electric to magnetic form factors is particularly sensitive to model details, as evident in Fig. V-1. This figure illustrates the dependence of the ratio on the strength of the lower component in the nucleon's wave function, which increases with increasing  $R$ . An article describing this work was published.<sup>1</sup>

\*Weierstrass Institute, Berlin, Germany.

<sup>1</sup>J. C. R. Bloch, A. Krassnigg, and C. D. Roberts, *Few Body Syst.* **33**, 219-232 (2003).

<sup>2</sup>M. K. Jones *et al.*, *Phys. Rev. Lett.* **84**, 1398 (2000).

<sup>3</sup>O. Gayou *et al.*, *Phys. Rev. C* **64**, 038202 (2001).

<sup>4</sup>O. Gayou *et al.*, *Phys. Rev. Lett.* **88**, 092301 (2002).

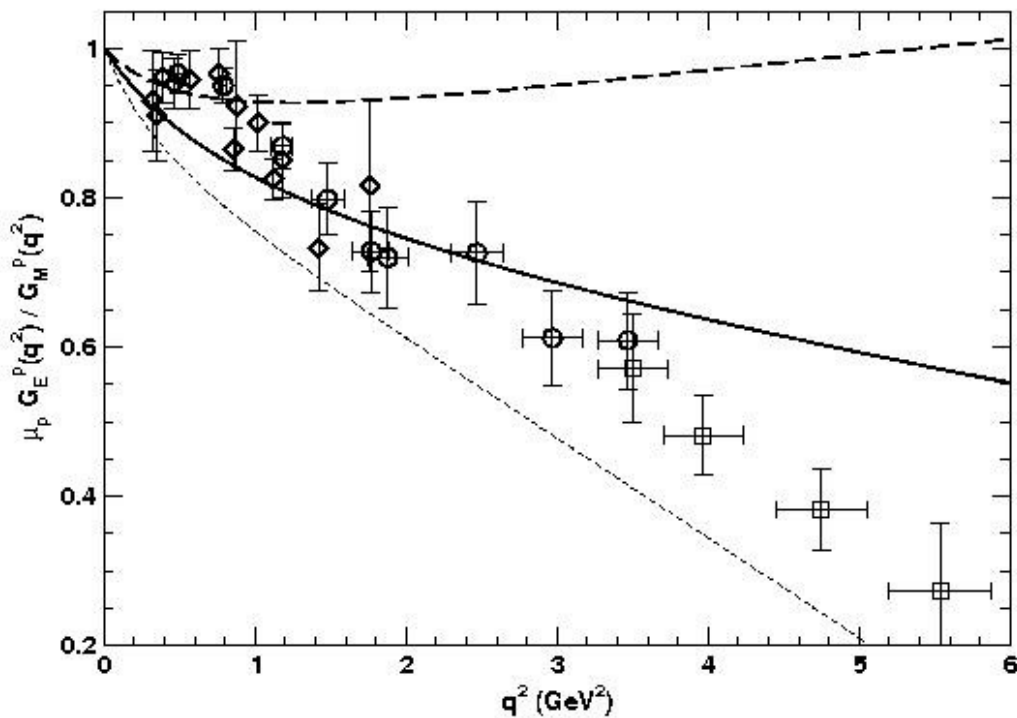


Fig. V-1. Calculated ratio  $\mu G_E^p(q^2)/G_M^p(q^2)$ : short-dash line,  $R=0$ ; solid line,  $R=0.25$ ; and dashed line,  $R=0.5$ . The strength of the lower component of the nucleon's rest-frame wave function increases with increasing  $R$ . The data are: boxes, Ref. [2]; diamonds, Ref. [3]; and circles, Ref. [4].

**a.7. Axial-Vector Diquarks in the Baryon** (R. Alkofer,\* A. Höll, M. Kloker,\*  
A. Krassnigg and C. D. Roberts)

A product *Ansatz* for the nucleon's Faddeev amplitude using only a scalar-diquark can provide a good description of leptonic and nonleptonic couplings and form factors, with some notable exceptions, *e.g.*, the neutron's charge radius and axial vector coupling. Properly incorporating the lower component of the nucleon's spinor helps somewhat in addressing these exceptions. However, discrepancies remain, and we

anticipate that their amelioration requires the inclusion of axial-vector diquark correlations and a pion cloud. We are exploring this with a view to quantifying the effects of these contributions on  $G_E^p(q^2)/G_M^p(q^2)$  and the  $N \rightarrow \Delta$  transition form factor. We have seen that the current body of data on both of these observables is dominated by nonperturbative dynamics.

\*University of Tübingen, Tübingen, Germany.

**a.8. Radially Excited Pseudoscalar Mesons** (A. Höll, A. Krassnigg, and  
C. D. Roberts)

A hallmark in the contemporary use of DSEs is the existence of a nonperturbative, symmetry preserving truncation scheme that enables the proof of exact results. For example, we have used this fact to demonstrate that the textbook value of the  $\pi^0 \rightarrow \gamma\gamma$  width is obtained algebraically and independent of model details if, and only if, a consistent truncation scheme is used.<sup>1</sup> Furthermore, we have proven that in the chiral limit the leptonic decay constant of every pseudoscalar meson, *except* that of the ground state pion, must vanish.<sup>2,3</sup> (NB. In a constituent-

quark model these pseudoscalar mesons are considered to be radial excitations of the ground state.) This exact result places a very tight constraint on all models and nonperturbative methods in their application to hadron spectroscopy and interactions, particularly in connection with the search for so-called exotic states in the 1-2 GeV range. We are currently employing a one-parameter model of the quark-quark interaction in a DSE study to illustrate this result and its corollaries.

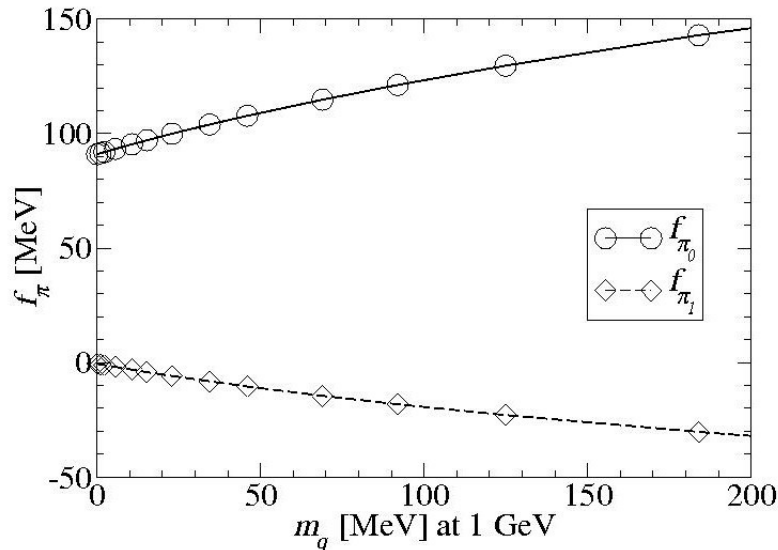


Fig. V-2. Calculated evolution of the leptonic decay constants with current-quark mass:  $\pi_0$ , ground state pion; and  $\pi_1$ , first radial excitation. In QCD, for all but the ground state the decay constant is precisely zero in the chiral limit as a consequence of dynamical chiral symmetry breaking.

This work provides the first Poincaré covariant and symmetry preserving analysis of meson excited states. Moreover it gives the first direct indication that when the current-quark mass is nonzero the leptonic decay constants of pseudoscalar mesons alternate in sign; viz., the decay constants of the ground state and the 2<sup>nd</sup>, 4<sup>th</sup>, etc. excited states are positive, while those of the 1<sup>st</sup>,

3<sup>rd</sup>, etc. are negative. *A posteriori* it is apparent that this outcome is necessary. Nevertheless, the result was not anticipated nor reported previously. We illustrate the evolution with current-quark mass of the leptonic decay constants of the ground state pion and its first excited state in Fig. V-2.

<sup>1</sup>A. Höll, A. Krassnigg, and C.D. Roberts, [nucl-th/0311033](https://arxiv.org/abs/nucl-th/0311033).

<sup>2</sup>A. Krassnigg and C. D. Roberts, [nucl-th/0308039](https://arxiv.org/abs/nucl-th/0308039).

<sup>3</sup>A. Krassnigg and C. D. Roberts, [nucl-th/0309025](https://arxiv.org/abs/nucl-th/0309025).

### a.9. Comparison of Point-Form Quantum Mechanics and Quantum Field Theory (F. Coester, A. Krassnigg, and C. D. Roberts)

We continue to explore the extent to which a relationship exists between bound state studies in relativistic quantum field theory and in relativistic quantum mechanics. Dyson-Schwinger equations provide a Poincaré covariant framework for continuum bound state studies in quantum field theory. In relativistic quantum mechanics, we adopt the point form because it, too, is manifestly covariant. In quantum mechanics one studies a mass operator and its eigenvalues. A key question is whether a mass operator and Hilbert space exist that can describe features equivalent to those obtained in quantum field theory. To be concrete, we will investigate axial-vector mesons

in both approaches. These states are particularly sensitive to long-range features of QCDs interaction, viz., aspects of confinement. A study of properties of the pion and its excited states is expected to answer interesting questions in both approaches. The dichotomous nature of the pion, as both a Goldstone mode and bound state of massive constituents, is likely to make a valid description in quantum mechanics impossible. Beyond two-particle systems we will investigate the nucleon in a constituent-quark Faddeev picture, concentrating on the dynamical properties of particle-exchange interactions.

### a.10. Scaling of Hadronic Form Factors in Point Form Kinematics<sup>1</sup> (F. Coester and D. O. Riska\*)

The calculation of hadronic form factors within the framework of Poincaré covariant quantum mechanics involves the following two separate ingredients: (1) bound-state wave functions, which represent vectors in the representation space of the little group of the Poincaré group, and (2) current operators that are covariant under a kinematic subgroup. Covariant conserved currents are generated from these ingredients by the dynamics, while the choice of the kinematic subgroup specifies the form of kinematics. Spectator currents, by definition, commute with quark spectator momenta, the definition of which depends on the choice

of a form of kinematics. Point-form kinematics employs the full Lorentz group as the kinematic subgroup. In this case the Lorentz covariant spectator currents probe the velocity structure specified by the bound-state wave function. When the extent of the wave function is scaled unitarily to zero (“point limit”), point-form kinematics yields a nontrivial scaling limit for the form factors, which depends on the shape of the wave function. Power-law model wave functions lead to a reasonable representation of the empirical form factors, while Gaussian wave functions fail.

\*University of Helsinki, Finland.

<sup>1</sup>Nucl. Phys. **A728**, 439 (2003).

### a.11. Baryon Form Factors of Relativistic Constituent-Quark Models<sup>1</sup> (F. Coester, B. Juliá-Díaz\* and D. O. Riska\*)

The electromagnetic and axial form factors of the nucleon and its lowest positive parity excitations, the  $\Delta(1232)$  and the  $N(1440)$ , are calculated with constituent-quark models that are specified by simple algebraic representations of the mass-operator eigenstates. Poincaré covariant current operators are generated by the dynamics from single-quark currents that are covariant under a kinematic subgroup. The dependence of the calculated form factors on the choice of kinematics and on the gross features of the wave functions is illustrated for instant-form, point-form, and front-form kinematics. A simple algebraic form of the

orbital ground state wave function, which depends on two parameters, allows a fair description of all the form factors over the empirically accessible range, although with widely different choices of the parameters, which determine the range and shape of the orbital wave function. The neutron electric form factor requires additional features, for instance the presence of mixed symmetry  $S$ -state component with 1-2% probability in the ground state wave function. Instant and front form kinematics demand a spatially extended wave function, whereas in point form kinematics the form factors may be described with a quite compact wave function.

\*University of Helsinki, Finland.

<sup>1</sup>To be published in Phys. Rev. C (2004).

### a.12. Electromagnetic Meson Production in the Nucleon Resonance Region (T.-S. H. Lee and V. Burkert\*)

A review article on the recent experimental and theoretical advances in investigating photo- and electro-production of mesons in the nucleon resonance region was completed. The article contains a comprehensive overview of all the existing experimental facilities with electron and photon beams, and also presents a unified derivation of most of the models being used to extract resonance parameters from the data. The investigations of the  $\Delta$  and  $N^*(1535)$  are discussed in detail, focusing on their interpretation in terms of current hadron

structure calculations, such as those from constituent quark models and lattice-QCD. The status of our understanding of reactions involving the production of kaons, vector mesons, and two pions is also reviewed. Finally, experimental developments in exploring whether the narrow-width  $\Theta^+$  peak observed recently in various reactions corresponds to a pentaquark is discussed. The paper will be published in International Journal of Modern Physics E.

\*Thomas Jefferson National Accelerator Facility.

### a.13. $\rho$ Meson Photoproduction at Low Energies (T.-S. H. Lee and Y. Oh\*)

The  $\sigma$ -exchange and  $f_2$ -exchange mechanisms for  $\rho$  meson photoproduction are re-examined. Then the commonly employed  $\sigma$ -exchange amplitude is revised by using recent information from analyses of the  $\rho \rightarrow \pi^0 \pi^0 \gamma$  decay and the  $\sigma NN$  coupling constant with the Bonn potential. Instead of relying of the Pomeron- $f$  proportionality assumption, the  $f_2$  meson exchange amplitude is established from an effective Lagrangian that is constructed from the tensor structure of the  $f_2$  meson. Phenomenological information together with tensor meson dominance and vector meson dominance assumptions are used to estimate the  $f_2$  coupling

constants. As a first step to improve the current theoretical models, we have also explored the effects of the un-correlated  $2\pi$  exchange amplitude with a  $\pi N$  intermediate state. This leading-order  $2\pi$  exchange amplitude can be calculated using coupling constants determined from the study of pion photoproduction and the empirical of  $\rho \rightarrow \pi\pi$  decay width. In comparing with existing differential cross section data, we find that a model with the constructed  $2\pi$ ,  $\sigma$ , and  $f_2$  exchanges (model B) is comparable to the commonly-used  $\rho$ -exchange model (model A) in which the  $\sigma$  coupling

\*Yonsei University, Korea.

<sup>1</sup>Y. Oh and T.-S. H. Lee, Phys. Rev. C **69**, 025201 (2004).

parameters are simply adjusted to fit the experimental data. The calculated differential cross sections from these two models are compared with the data in Fig. V-3. We suggest that experimental verification of the predicted single and double spin asymmetries in the small  $|t|$  ( $<2 \text{ GeV}^2$ ) region will be useful for

distinguishing the two models and improving our understanding of the non-resonant amplitude for  $\rho$  photoproduction. Possible further improvements of the model are discussed. A paper describing our results was published.<sup>1</sup>

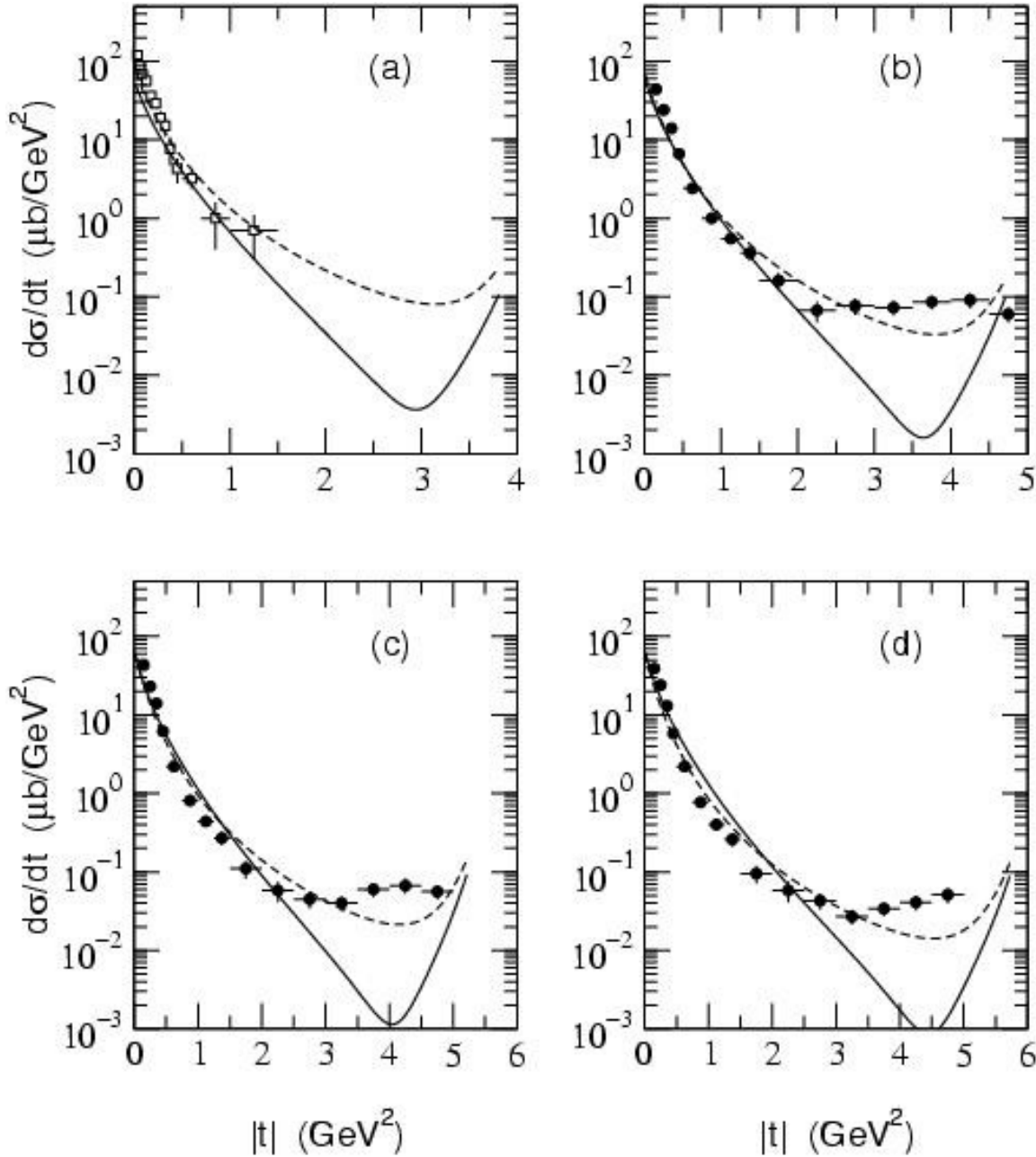


Fig. V-3. Differential cross sections  $\gamma p \rightarrow \rho^0 p$  at  $E_\gamma =$  (a) 2.8, (b) 3.28, (c) 3.55, and (d) 3.82 GeV. The dashed lines are the results of model A and the solid lines are those of model B.

### a.14. Dynamical Coupled-Channel Model of Kaon-Hyperon Interactions

(T.-S. H. Lee, W.-T. Chiang,\* B. Sashai,† and F. Tabakin‡)

The  $\pi N \rightarrow KY$  and  $KY \rightarrow KY$  reactions are studied using a dynamical coupled-channel model of meson-baryon interactions at energies where the baryon resonances are strongly excited. The channels included are:  $\pi N$ ,  $K\Lambda$ , and  $K\Sigma$ . The resonances considered are:  $N^*$  [ $S_{11}(1650)$ ,  $P_{11}(1710)$ ,  $P_{13}(1720)$ ];  $\Delta^*$  [ $S_{31}(1900)$ ,  $P_{31}(1910)$ ,  $P_{33}(1920)$ ];  $\Lambda^*$  [ $S_{01}(1670)$ ,  $P_{01}(1810)$ ];  $\Sigma^*$  [ $P_{11}(1660)$ ,  $D_{13}(1670)$ ]; and  $K^*(892)$ . The basic non-resonant  $\pi N \rightarrow KY$  and  $KY \rightarrow KY$  transition potentials are derived from effective Lagrangians using a unitary transformation method. The dynamical coupled-channel equations are simplified by parametrizing the  $\pi N \rightarrow \pi N$  amplitudes in terms of empirical  $\pi N$  partial-wave amplitudes and a phenomenological off-shell

function. Two models were constructed. Model A is built by fixing all coupling constants and resonance parameters using SU(3) symmetry, the Particle Data Group values, and results from a constituent quark model. Model B is obtained by allowing most of the parameters to vary around the values of model A in fitting the data. Good fits to the available data for  $\pi p \rightarrow K^0\Lambda$ ,  $K^0\Sigma$  were achieved. The investigated kinematical region in the center-of-mass frame goes from threshold to 2.5 GeV. One of our results is shown in Fig. V-4. The constructed models can be embedded in associated dynamical coupled-channel studies of kaon photo- and electro-production reactions. A paper describing our results was submitted for publication.

\*Institute of Physics, Academia Sinica, Taiwan, †CEA/Saclay, France, ‡University of Pittsburgh.

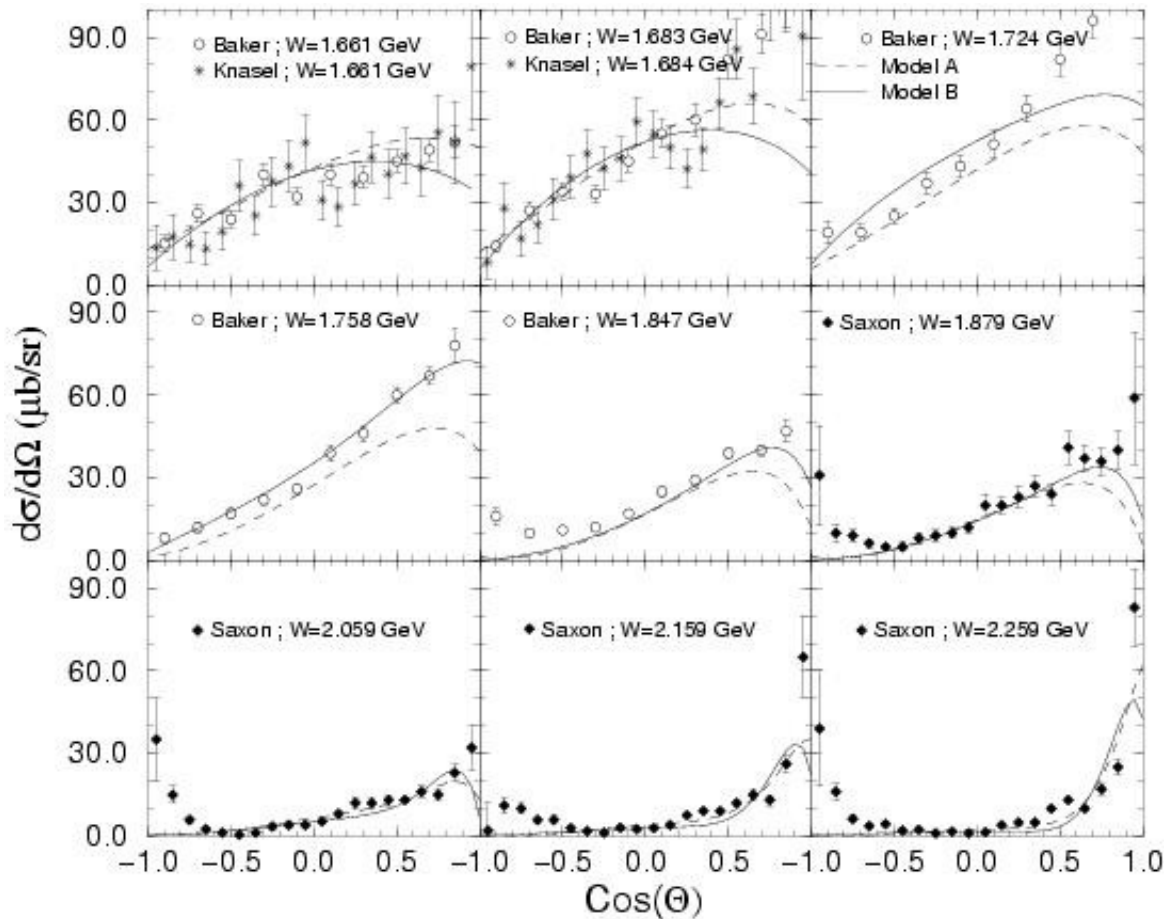


Fig V-4. Differential cross-section for the reaction  $\pi p \rightarrow K^0\Lambda$ . The curves are from models A (dashed curves) and B (full curves).

### a.15. Coupled-Channel $\pi\pi N$ Model for Meson Production Reactions (T.-S. H. Lee, A. Matsuyama,\* and T. Sato†)

For investigating the structure of nucleon resonances ( $N^*$ ) using the very extensive data from Jefferson Laboratory, we extended our dynamical model (Sato-Lee Model) for the  $\Delta$  excitation to include additional meson-baryon channels ( $\eta N$ ,  $\omega N$ , etc.) and the three-body  $\pi N$  ( $\pi\Delta$ ,  $\rho N$ ) channels. The resulting Faddeev-type coupled-channel scattering equations are solved by using the Spline-Function method such that the  $\pi\pi N$  cut effects can be included exactly in calculating the meson production cross sections. This crucial numerical advance has overcome the main difficulty in all the previous works using the method of contour rotation.

The multipole amplitudes associated with the  $\pi N$   $S_{11}$  channel can be described in a calculation including  $\gamma N$ ,  $\pi N$ ,  $\eta N$ , and  $\pi\pi N$  ( $\pi\Delta$ ) channels. The resonance parameters of  $N^*(1535)$  and  $N^*(1650)$  were extracted from the data. Our sample results for  $\pi N$  scattering and  $\gamma N \rightarrow \pi N$  up to  $W = 2$  GeV are shown in Fig. V-5. Our main finding is that meson cloud effects can change the  $\gamma N \rightarrow N^*(1535)$  amplitude by about 20%. This is consistent with our result in the study of the  $\Delta$  resonance. Work on other partial waves is in progress.

\*Schizuoka University, Japan, †Osaka University, Japan.

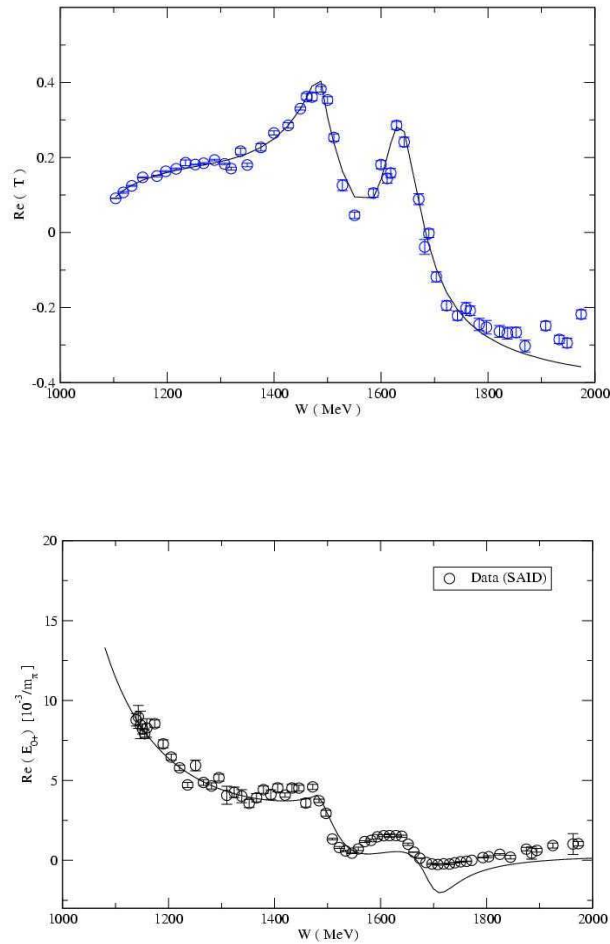


Fig V-5. The real parts of the multipole amplitudes for  $\pi N \rightarrow \pi N$  (upper part) and  $\gamma N \rightarrow \pi N$  (lower part) reactions in the  $S_{11}$  channel.

### a.16. Light-Front Quark Model Calculations of $\gamma N \rightarrow \Delta$ Form Factor (T.-S. H. Lee and T. Sato\*)

Within the Sato-Lee model, we had extracted the  $\gamma N \rightarrow \Delta$  form factors from JLab pion electroproduction data. It was found that the pion cloud effects are very large and the resulting bare form factors can be identified with the constituent quark model predictions at  $Q^2 = 0$ , the real photon point. Our objective in this work is to explore the extent to which such agreement can also be verified in the whole considered range of  $Q^2 < 5$  (GeV/c)<sup>2</sup>. As a first step, we extended the light-front calculation of Schlemf to include the  $\Delta$  excitation. Our nucleon form factor results are comparable to those of Miller who also used the model of Schlemf. In Fig.

V-6, the predicted  $\gamma N \rightarrow \Delta$  M1 form factor is compared with the "data" extracted within the Sato-Lee model. We see that the predictions are sensitive to the range parameter,  $a$ , of the quark wavefunction. With the value  $a = 0.607$ , which gives good nucleon form factor results, the prediction (solid curve) deviates significantly from the data. The prediction can be greatly improved if we use a smaller range  $a = 0.507$ . We are in the process of exploring how such a wavefunction can be obtained from a constituent quark model.

\*Osaka University.

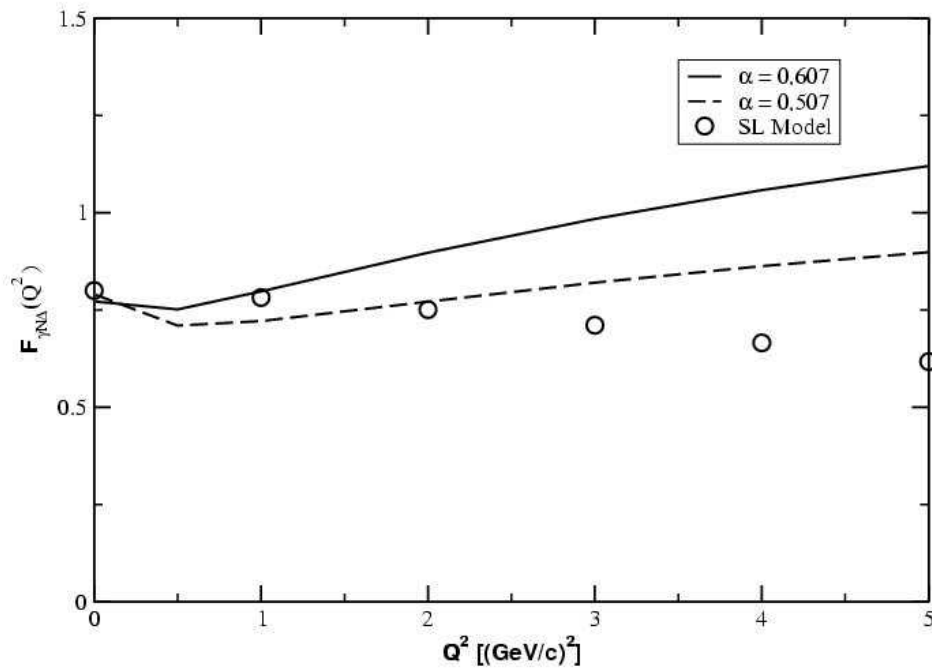


Fig. V-6. Light front calculation of  $\gamma N \rightarrow \Delta$  M1 form factors. The data are the bare form factor extracted from pion electroproduction data within the Sato-Lee model. "a" is a range parameter of the constituent quark wavefunction within the model of Schlemf.

### a.17. Study of the Parity of the $\Theta^+$ Resonance Peak with ${}^3\overline{\text{He}} (\vec{\gamma}, K^+ K^- n)$ Reaction (T.-S. H. Lee, X. Zheng, and Y. Oh\*)

One of the crucial quantities for determining whether the narrow-width resonance peak (called  $\Theta^+$ ) observed recently in various reactions corresponds to a pentaquark state is its parity. By performing calculations using the  $\Theta^+$  production model of Oh, we have found that the parity of the  $\Theta^+$  can be decisively determined by measuring the double polarization observables of the kaon photoproduction reaction  $\vec{\gamma} + \bar{n} \rightarrow K^+ + K^- + n$ . We focus on the differential cross sections with all three final particles,  $K^+$ ,  $K^-$ , and neutron, detected in coincidence. The predicted photon

asymmetries at  $\theta_{K^-} = 30^\circ$ , as a function of the angle of  $K^+$ , are compared in Fig. V-7. Here, the initial neutron is polarized in the opposite direction to the incident photon. The photon is circularly polarized. This double spin observable is obviously very useful for distinguishing the parity of the  $\Theta^+$  peak. We are in the process of applying the model to make predictions for a realistic experiment with a polarized  ${}^3\text{He}$  target. Effects due to the non- $\Theta^+$  production mechanisms will also be investigated.

\*University of Georgia.

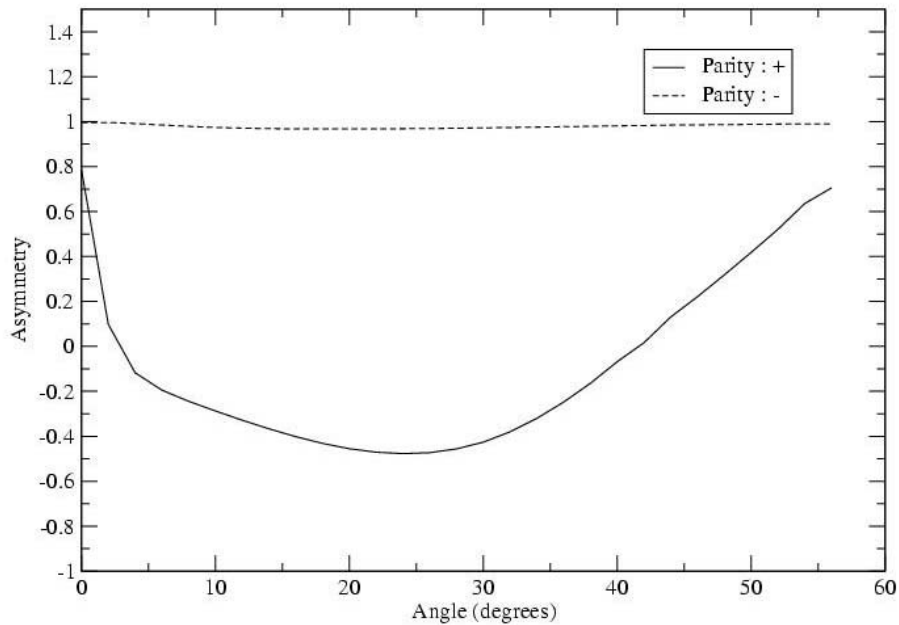


Fig. V-7. Dependence of the photon asymmetries in the  $\vec{\gamma} + \bar{n} \rightarrow K^+ + K^- + n$  reaction on the parity of the intermediate  $\Theta^+$  state. The  $K^-$  is detected at a fixed angle  $\theta_{K^-} = 30^\circ$ . The angles on the x-axis denote the directions of the detected  $K^+$ . The initial neutron is polarized in the opposite direction to the incident photon. The photon is circularly polarized.

### a.18. Medium Effects in the Electromagnetic $\rho$ Meson Production on Nuclei (T.-S. H. Lee, Y. Oh,\* and R. Rapp†)

The medium effects on vector meson propagation in nuclear matter were found to be crucial in understanding the dilepton production from relativistic heavy-ion collisions. In particular, the medium effects predicted by Rapp and Wambach provided a quantitative explanation of the dilepton production data

without invoking the assumption that the quark-gluon plasma was created during the collisions. On the other hand, the predicted medium effects must be verified in other reactions which do not have the complexities of relativistic heavy-ion collisions. We are carrying out such an investigation by considering the

photoproduction of  $\rho$  mesons on nuclei. The  $\rho$  photoproduction amplitude is generated from the model of Oh and Lee, and the in-medium  $\rho$  propagator is generated from the model of Rapp and Wambach. We first perform a calculation in nuclear matter. The results are shown in Fig. V-8. We see that medium effects can drastically reduce the magnitudes and change the shapes of the production cross sections. We

are now developing a reaction model to make predictions for  $\rho$  photo- and electro-production on finite nuclei, in order to compare with the data from Jefferson Laboratory. Our prediction will also be the baseline for exploring color transparency using the data which have recently been obtained by the Argonne Medium Energy group.

\*University of Georgia, †Texas A&M University.

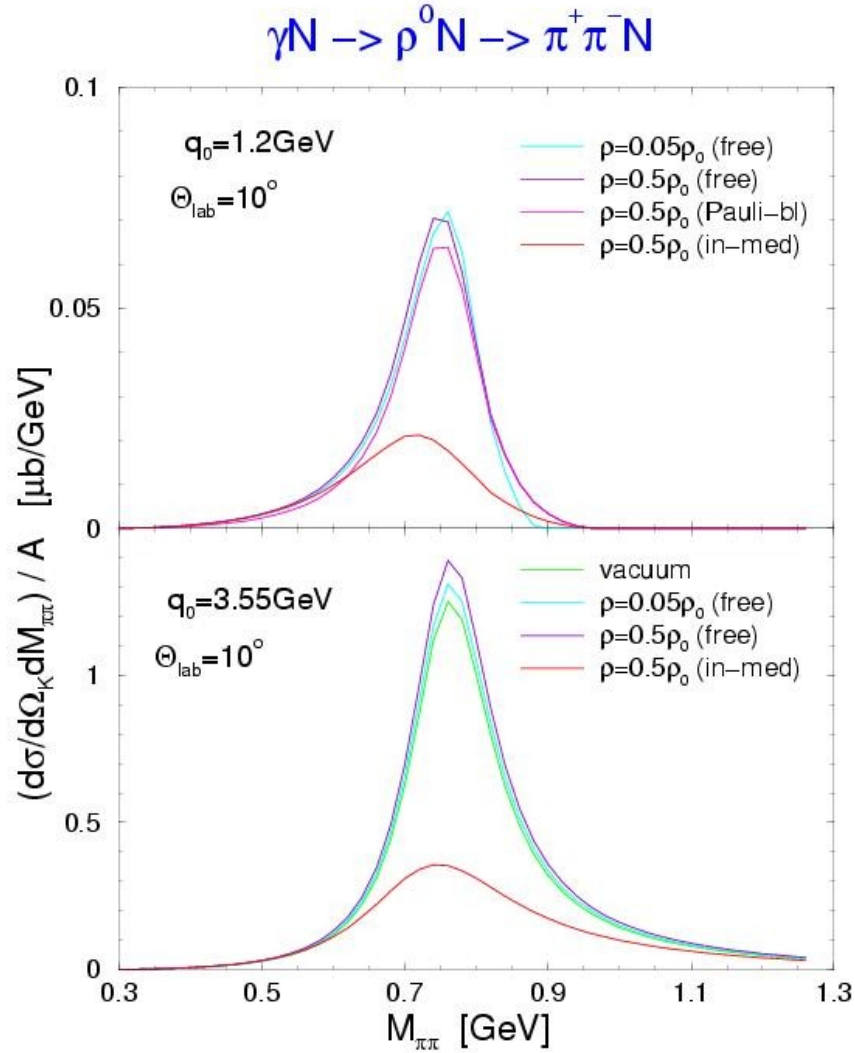


Fig. V-8. The two-pion spectra from  $\gamma p \rightarrow \rho p$  reaction in nuclear matter.  $\rho_0$  is the usual nuclear matter density.  $q_0$  is the photon energy.  $\theta_{lab}$  is the angle between the outgoing  $\rho$  and incoming  $\gamma$ .  $M_{\pi\pi}$  is the invariant mass of the detected two pions.

### a.19. Particle Ratios at RHIC and Chemical Freeze-Out (S. Schramm, D. Zschesche,\* H. Stöcker,\* and J. Schaffner-Bielich†)

We investigated hadronic particle production in ultrarelativistic heavy-ion collisions at RHIC. Thermodynamical equilibrium calculations of particle production in high energy particle- and nuclear collisions have been carried out for a long time. Experimental data for hadron abundances and ratios have been obtained in heavy-ion collisions at the SIS, AGS, SPS and more recently at the RHIC facility.

The plethora of data revived interest in extracting a common temperature and chemical potential for the chemical freeze-out point that determines the particle ratios using a thermal equilibrium model analysis. The experimentally determined hadron ratios can be fitted quite well with simple non-interacting gas models, if a sudden breakup of a thermalized source is assumed and the subsequent feeding of the various channels from strongly decaying higher resonances is taken into account. From the  $\chi^2$  freeze-out fits one has constructed a quite narrow band of freeze-out values in the  $T$ - $\mu_B$  plane. The extracted freeze-out parameters are close to the assumed phase transition curve for SPS and RHIC energies. However, if the system passes through the vicinity of the phase transition (or through the crossover range) as suggested by the data for  $T$  and  $\mu_B$ , one cannot neglect the in-medium effects that are responsible for the phase transition in the first place. Thus, non-interacting gas models, as they completely neglect any kind of possible in-medium modification, can only yield limited insight. Therefore, we based our studies on a relativistic self-consistent hadronic 3-flavor model. One can view the model as a thermodynamically consistent effective theory or as a toy model that includes the restoration of chiral symmetry at high temperatures or densities. In either case the model incorporates temperature and density dependent hadronic masses and effective chemical potentials.

Depending on the chosen parameters and degrees of freedom, different scenarios for the chiral phase change are predicted by the model: strong or weak first order phase transition, or a crossover. The transitions take

place around  $T_c = 155$  MeV, in qualitative agreement with lattice estimates of the critical temperature for the onset of a deconfined and chirally restored phase.

A whole range of particle ratios are calculated in the SU(3) model and compared with the RHIC data for Au + Au at  $\sqrt{130}$  AGeV. In addition a comparison with non-interacting gas calculations was performed.

Since different parametrizations of the model show qualitatively different phase transition scenarios, we investigate whether the particle production, *i.e.*, the chemistry of the system, is sensitive to the phase transition behavior. Since we have shown that the current data are described by all three different phase transition scenarios (strong first order, weak first order or smooth crossover) and the ideal gas model, we can so far neither favor nor rule out any one scenario.

In all interacting models the effective masses at freeze-out are shifted by up to 15% from their vacuum values. The fit values for the chemical freeze-out temperature and chemical potential depend on the order of the phase transition. The crossover case yields temperatures that are shifted by 15 MeV as compared to the non-interacting gas model while the model calculations with a first order phase transition show more than 30 MeV lower temperatures.

Strikingly, the fitted freeze-out points are located very close to the phase transition boundary in the first-order phase transition scenarios, but  $T$  is always smaller than  $T_c$ . This suggests that at RHIC the system emerges after passing through the chiral phase transition. This of course is only true if a first order phase transition does actually occur in QCD at small chemical potentials and high  $T$ . Furthermore, from our studies it becomes clear that a "freezing" of the relative abundances of various hadrons in the symmetric phase (at  $T > T_c$ ) is definitely excluded.

An article describing aspects of this work was published.<sup>1</sup>

\*University of Frankfurt, †Brookhaven National Laboratory.

<sup>1</sup>D. Zschesche, G. Zeeb, K. Paech, H. Stöcker, and S. Schramm, J. Phys. G **30**, 5381-5391 (2004).

## B. NUCLEAR FORCES AND NUCLEAR SYSTEMS

The goal of this program is to achieve a description of nuclear systems ranging in size from the deuteron and triton to nuclear matter and neutron stars using a single parametrization of the nuclear forces. Aspects of our program include both the construction of two- and three-nucleon potentials and the development of many-body techniques for computing nuclear structure and reactions with these interactions. Detailed quantitative, computationally-intensive studies are essential parts of this program.

Quantum Monte Carlo (QMC) calculations of light ( $A \leq 12$ ) nuclei with realistic interactions have been the main focus of our recent efforts. Our nonrelativistic Hamiltonian contains the accurate Argonne v18 two-nucleon ( $NN$ ) potential, which includes charge-independence breaking terms, and either the venerable Urbana IX three-nucleon ( $NNN$ ) potential, or one of several Illinois  $NNN$  models. The QMC calculations include both variational (VMC) and Green function (GFMC) methods. We begin with the construction of variational trial functions based on sums of single-particle determinants with the correct total quantum numbers, and then act on them with products of two- and three-body correlation operators. Energy expectation values are evaluated with Metropolis Monte Carlo integration and parameters in the trial functions are varied to minimize the energy. These optimized variational wave functions can then be used to study other nuclear properties. They also serve as a starting point for the GFMC calculations, which systematically remove higher excited-state components from the trial wave functions by propagation in imaginary time.

We are currently studying all  $A \leq 10$  nuclei, including more than 80 ground or excited states, and the ground state of  $^{12}\text{C}$ . These are the first calculations treating  $A \geq 6$  nuclei directly with realistic  $NN$  and  $NNN$  interactions. In GFMC calculations, with the Illinois  $NNN$  models, we can reproduce most of the experimental ground- and excited-state energies within 0.7 MeV. Recently we found that GFMC propagation, started with orthogonalized VMC wave functions for multiple states of the same spin and parity, preserves the orthogonality to a very good approximation. This enables the calculation of many more states for  $A \leq 10$ ; in previous years only some 30 states were done. We are also studying the properties of neutron drops with the goal of modeling neutron-rich isotopes of nuclei, such as oxygen, out to the neutron drip line.

This year we made a study of different forms for the quadratic momentum dependence in the  $NN$  interaction by constructing an alternate version of the Argonne v18  $NN$  potential. Instead of partial-wave local  $L^2$  terms, we used nonlocal  $p^2$  terms, as well as a different form of quadratic spin-orbit operator, to refit the  $NN$  phases in a model we designate Argonne v18pq. VMC calculations of few-body nuclei with the two models, and with various  $NNN$  potentials added, show no significant change in the predicted nuclear binding. Adapting the GFMC algorithm to handle a potential like v18pq is not trivial; the present study does not encourage us to make such an effort.

### b.1. Quantum Monte Carlo Calculations of Light p-Shell Nuclei (S. C. Pieper, R. B. Wiringa, J. Carlson,\* V. R. Pandharipande,† and K. Varga‡)

Since the early 1990s, we have been studying the ground and low-lying excited states of light p-shell nuclei as  $A$ -body problems with realistic nucleon-nucleon ( $NN$ ) and three-nucleon ( $NNN$ ) interactions using advanced quantum Monte Carlo (QMC) methods. Our preferred Hamiltonians contain the Argonne  $v_{18}$   $NN$  potential (AV18), which gives an excellent fit to elastic  $NN$  scattering data and the deuteron energy, and the Illinois  $NNN$  potentials, which we have fit to binding energies of  $A \leq 8$  nuclei. The QMC methods include both variational Monte Carlo (VMC), which gives an initial approximate solution to the many-body Schrödinger equation, and Green function Monte Carlo (GFMC), which systematically improves on the VMC starting point and produces binding energies that are accurate to within 2%. In this year we have revisited our  $A = 6$ --8 calculations and added calculations of multiple states with the same quantum numbers in these nuclei. We have also continued preliminary calculations of  $^{12}\text{C}$ .

The VMC calculations begin with the construction of an antisymmetric Jastrow trial wave function that includes single-particle orbits coupled to the desired  $JM$  values of the state of interest as well as pair and triplet spatial correlations. It is then acted on by a symmetrized product of two-body spin, isospin, and tensor correlation operators, induced by the  $NN$  potential, and three-body correlation operators for the  $NNN$  potential. The wave functions are diagonalized in the small basis of different Jastrow spatial symmetry

components to project out higher excited states with the same quantum numbers.

In the GFMC calculations, we operate on a version of the VMC trial function with the imaginary time propagator,  $\exp[-(H'-E_0)\tau]$ , where  $H'$  is a simplified Hamiltonian,  $E_0$  is an estimate of the eigenvalue, and  $\tau$  is the imaginary time. The excited-state components of the trial function will then be damped out for large  $\tau$ , leaving the exact lowest eigenfunction with the quantum numbers of the input variational wave function. The expectation value of  $H$  is computed for a sequence of increasing values of  $\tau$  to determine the convergence. Our  $H'$  contains a simplified, reprojected eight-operator version of the  $NN$  potential, AV8', and the full  $NNN$  potential. The small correction,  $H-H'$ , is computed perturbatively. The many-body propagator is written as a symmetrized product of exact two-body propagators, with the  $NNN$  potential treated in lowest order.

In previous years we made significant improvements in the GFMC algorithms, especially in solving the fermion sign problem for nuclear systems. The main technical advances made this year were to use Monte Carlo sampling of nucleon pairs for the evaluation of the  $L^2$  terms in the Hamiltonian and of nucleon triples for the three-nucleon potential. This has resulted in a significant speedup of calculations of larger nuclei.

Our recent QMC work is described in the following subsections.

\*Los Alamos National Laboratory, †University of Illinois, Urbana, ‡Oak Ridge National Laboratory.

### b.2. Recent Progress in Quantum Monte Carlo Calculations (S. C. Pieper, R. B. Wiringa, and J. Carlson\*)

Last year we made extensive tests of the reliability of GFMC propagation for larger nuclei, particularly considering the new  $NNN$  terms in the Illinois potentials. We found that the scheme that had been developed for the Urbana  $NNN$  potentials was less reliable for the new potentials. Using the complete  $NNN$  potential in the propagation appeared to be the only solution, but this requires an increasing fraction of the total time as the size of the nucleus is increased. This year we developed a sampling technique for three-body clusters to choose only a subset of the  $A(A-1)(A-2)/6$  clusters when computing the  $NNN$  potential or

propagator. We find very good results with as few as only 15% of the triples. With this method, the  $NNN$  potential and propagator now contribute only 20% of the total time in a  $^{12}\text{C}$  calculation, and a smaller fraction in lighter nuclei.

Another time-consuming part of the Monte Carlo calculations is the evaluation of the expectation values of the  $L^2$  and  $(L \cdot S)^2$  potentials. These require three wave function evaluations for each  $NN$  pair. But these potentials are quite short-ranged so again we find that

sampling of the pairs works well; evaluation of only 20% of the pairs gives better than 1% accuracy.

In 2002 we found that GFMC can be used to compute higher excited states with the same quantum numbers as lower states if the propagation is started with a trial wave function that is orthogonal to the starting wave function for the lower state. We have been systematically computing all states that are typically identified as P-shell states in  $A = 6, 7, 8$  nuclei. We have also been repeating our old calculations of these nuclei using just the AV18 and AV18 + UIX Hamiltonians. In some cases we have found results that are several percent different from our published values; these differences are mostly due to the difficulties of making

adequate calculations or tests on the slower computers of five years ago. This work will be submitted for publication soon.

At the very beginning of 2003, we made our first GFMC calculations of  $^{12}\text{C}$  on Argonne's new Jazz computer. Simplified starting wave functions and  $NNN$  propagation were used. We have developed a starting wave function based on a complete p-shell description of  $^{12}\text{C}$  and used it to make a more reliable calculation with just two-nucleon forces. This GFMC calculation used some 75,000 processor hours on the Los Alamos qsc computer. We will use our improved  $NNN$  propagation method to make a calculation including the Illinois-2  $NNN$  potential this coming year.

\*Los Alamos National Laboratory.

### **b.3. Pairing and Spin-Orbit Splitting in Neutron Drops (S. C. Pieper and V. R. Pandharipande\*)**

Systems of neutrons interacting with realistic forces are unbound. However, bound systems may be made by adding an artificial external well to the Hamiltonian. These may then be used to study spin-orbit splitting and pairing energies in neutron-rich systems and to possibly provide "experimental" energies to help constrain Skyrme models for large neutron-rich nuclei. A number of years ago we published results for 7 and 8 neutrons interacting via AV18 + Urbana IX in an external well and the corresponding 6-neutron system was also published.

This year we constructed a well such that the differences of the binding energies of 8-, 9-, and 10-neutron drops, computed using the well with the AV18 + IL2 interaction, are close to the corresponding differences of the binding energies of  $^{16,17,18}\text{O}$ . Thus the well is supposed to mimic the protons in the core of neutron-rich oxygen isotopes. The energies of up to 14

neutrons with this Hamiltonian have been computed and, as shown in Fig. V-9, closely track the energies of the oxygen isotopes. The main deficiency seems to be that the computed  $d_{5/2} - d_{3/2}$  spin-orbit splitting is too small compared to the experimental oxygen splittings. We will probably have to include a one-body spin-orbit potential in the definition of the well to improve this feature. We intend to compute the 16-neutron system (which is becoming a substantial calculation), and perhaps the 18-neutron one, to see if we can reproduce the neutron-drip line for oxygen. We also intend to look at the energies of  $2^+$  states for these drops.

The calculation of the neutron drops with more than 9 neutrons is made possible by using a BCS wave function. This wave function introduces 1s, 1p, 2s, and 1d pairs but does not differentiate between  $d_{5/2}$  and  $d_{3/2}$  pairs. This could be an important deficiency that we intend to address.

\*University of Illinois, Urbana-Champaign.

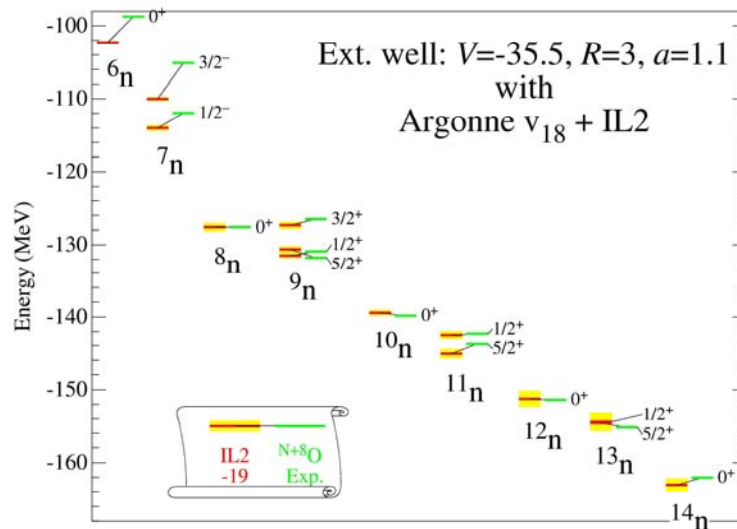


Fig. V-9. Energies of neutron systems interacting with the described Hamiltonian compared to the experimental energies of oxygen isotopes. The computed energies have all been shifted by 19 MeV to match the 8-neutron drop energy to the experimental  $^{16}\text{O}$  energy.

#### b.4. Quadratic Momentum Dependence in the Nucleon-Nucleon Interaction

(R. B. Wiringa, A. Arriaga,\* and V. R. Pandharipande†)

Modern nucleon-nucleon ( $NN$ ) interactions start with eight basic operators, including central, spin-spin, tensor, and spin-orbit terms, and each of these times isospin. With these operators it is possible to fit S- and P-wave phase shifts and deuteron properties reasonably well, as has been done with the Argonne  $v_8'$  (AV8') potential. However, to fit higher partial waves, *e.g.*, the difference between  $^1S_0$  and  $^1D_2$  partial waves, it is necessary to add operators with a quadratic momentum dependence (QMD). An example of this is the use of four  $L^2$  and two  $(L.S)^2$  operators in the Argonne  $v_{18}$  (AV18) potential.

There are other possible choices for the QMD terms, *e.g.*,  $p^2$  instead of  $L^2$  operators, and different kinds of quadratic spin-orbit terms. One advantage of the AV18 structure is that the potential is local, since  $L^2$  commutes with functions of radial coordinates. However, potentials based on field-theoretic models of meson exchange are more likely to have  $p^2$  terms, as in the Bonn, Nijmegen, and Paris potentials. The  $p^2$  operator does not commute with radial functions and consequently such models are nonlocal; they are also somewhat harder to evaluate with our quantum Monte Carlo many-body methods. Nevertheless, there is some indication in the literature that such nonlocal potentials

may provide increased attraction in light nuclei such as  $^3\text{H}$  and  $^4\text{He}$ .

We investigated the effect of such nonlocality in the  $NN$  potential by constructing an alternate, phase-equivalent version of the AV18 potential, designated AV18pq, in which the  $L^2$  and  $(L.S)^2$  terms were replaced by  $p^2$  and  $Q_{ij}$  operators, respectively. However, the strength of these terms was not imposed by some field-theoretic model, but was determined by the empirical need to fit  $NN$  data. The resulting QMD terms are smaller in this new potential than in AV18, while the deuteron wave function is somewhat larger at short distance. Variational Monte Carlo calculations of  $^3\text{H}$ ,  $^3\text{He}$ , and  $^4\text{He}$  binding energies show very little difference between the two models, with the nuclei underbound compared to experiment. When a realistic three-nucleon (3N) potential such as Urbana IX or Tucson-Melbourne is added, the binding approaches the experimental value, but AV18pq gains slightly less binding than AV18 for the same 3N force.

The first four operator components of the two potentials, *i.e.*, the central, isospin, spin, and spin-isospin parts, are shown in Fig. V-10. It is interesting to note that the short-range behavior of the spin- and

isospin-dependent terms can be significantly modified by the choice of the QMD terms. However, it appears that this kind of nonlocality has little practical effect on

ground state energies. This work was published during the year.<sup>1</sup>

\*University of Lisbon, Portugal, †University of Illinois at Urbana-Champaign.

<sup>1</sup>R. B. Wiringa, A. Arriaga, and V. R. Pandharipande, Phys. Rev. C **68**, 054006 (2003).

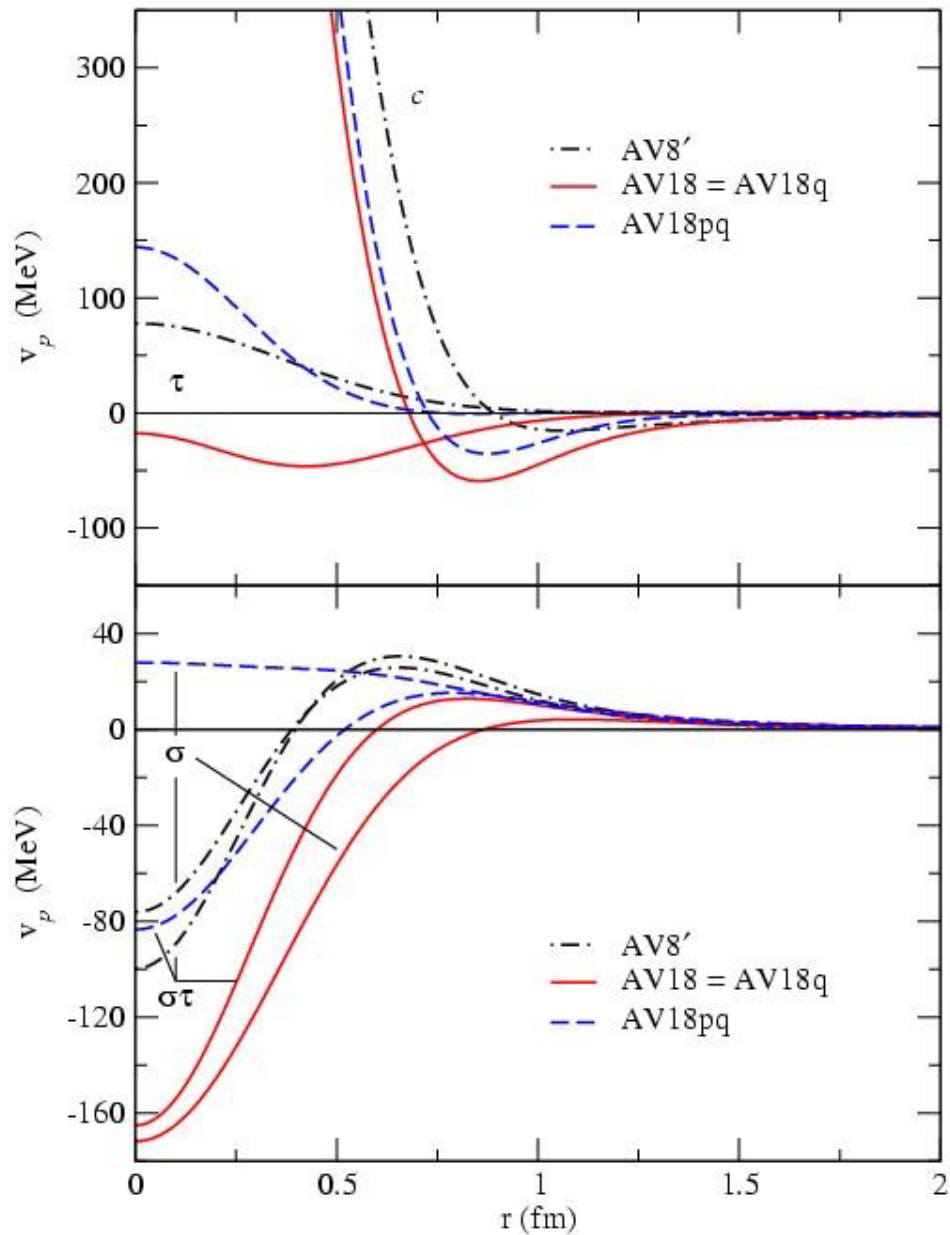


Fig. V-10. Leading operator components of the AV8', AV18, and AV18pq potentials.

### C. NUCLEAR ASTROPHYSICS

The objective of this research program is to investigate nuclear processes that take place in stars, in the big bang, and in interstellar and intergalactic space. Nuclear phenomena are ubiquitous in the universe. The stars shine by nuclear energy, and the chemical compositions observed in the solar system and elsewhere are the results of nuclear processes that occurred in the big bang and inside the several generations of stars that have formed since then. Many astrophysical phenomena may only be understood by a combination of nuclear physics with methods more familiar to astrophysicists.

A particularly important problem is to determine rates for the nuclear reactions that occur in astrophysical environments. We have applied advances in the theoretical descriptions of light nuclei to compute cross sections important for big-bang nucleosynthesis and the solar neutrino flux. This work continues in close connection with our other work on light nuclei, and the main goals at present are to improve the wave functions and computational methods. There are many applications (for example, the rapid neutron capture process) where large contributions from theoretical nuclear physics – particularly masses and cross sections – will always be necessary as input, and we maintain research interests in these areas.

Understanding nucleosynthesis and energy generation in a particular astrophysical environment requires calculations of nuclear reaction networks. Even for cases in which the detailed astrophysical phenomena can only be understood from difficult calculations coupling a reaction network and hydrodynamics, simpler network calculations can identify the crucial reactions and other nuclear properties to be determined by more detailed theoretical and experimental work. Ongoing work in this area involves big-bang nucleosynthesis, nuclear burning in low-mass stars, and photon-nucleus reactions in high-energy cosmic rays.

A major goal of nucleosynthesis studies is to determine the specific physical conditions that gave rise to abundance patterns seen in nature: what mix of different kinds of stellar environments gave rise to observed chemical compositions? Large amounts of important new data on abundance patterns are now being collected, with important evidence arising from low-metallicity stars in our own galaxy, absorption-line systems backlit by distant quasars, and primitive inclusions and pre-solar grains embedded in meteorites. These data contain important clues about the nucleosynthetic history of the universe, both locally and globally, and the effort to disentangle the clues into information on stellar sources and galactic chemical evolution is necessarily coupled to our work on nucleosynthesis.

### c.1. Mixing in AGB Stars and Radioactivities in the Early Solar System

(K. M. Nollett, M. Busso,\* R. Gallino,<sup>†</sup> and G. J. Wasserburg<sup>‡</sup>)

Sun-like stars, with masses below  $3M_{\odot}$ , are important sources of nuclei. They produced about half the nuclei heavier than iron in the solar system, a large fraction of the carbon, and possibly most of the nitrogen. In addition, the most numerous category of pre-solar grains recovered from meteorites, the “mainstream” grains, almost certainly formed in the ejecta from such stars.

Composition data from the meteorite grains and from astronomical observations suggest that there are mixing processes inside low-mass stars during the final red giant branch and asymptotic giant branch (AGB) stages, in addition to those processes present in standard one-dimensional stellar evolution models. We previously<sup>1</sup> computed the effects of slow mixing of composition between the convective envelope of a  $1.5M_{\odot}$  star and the hotter layers below, during the final few million years of the star's existence on the AGB. This process is referred to as “extra mixing” or “cool bottom processing” (CBP). The calculations showed that without severely disrupting the star's energy budget, composition patterns in the oxygen isotopes found in pre-solar oxide grains may be explained. If mixing is sufficiently deep, the abundances of the short-lived  $^{26}\text{Al}$  incorporated into oxide grains may be explained. There are also important consequences for the formation of carbon stars and the subsequent planetary nebulae, since much of the carbon produced in the star's helium shell may subsequently be converted into nitrogen by the slow mixing.

Since the radioactive  $^{26}\text{Al}$  may be produced by CBP, there are also important consequences for the sources of the radionuclides known to have been present in meteorites that formed when the solar system first

condensed. There has long been a puzzle as to how much of the early solar system inventory of radionuclides came from various sources. Sources for radionuclides include input from a nearby supernova or AGB star just before the solar system condensed, production from ions accelerated by the magnetic field of the sun during its formation, or simply from accumulated nucleosynthesis by many generations of stars. To determine the viability of a single AGB source for the nuclides with lifetime less than about 10 Myr, the  $^{26}\text{Al}$  yield of these stars is crucial. Without CBP, these stars should make a small amount of  $^{26}\text{Al}$  in the hydrogen-burning shell, but then destroy much of it by exposure to neutrons in the helium shell. The  $^{26}\text{Al}$  yield deposited in the interstellar medium is then tied to the amount of helium-shell material dredged to the stellar surface. The AGB source model has previously been constrained by a combination of the  $^{26}\text{Al}$  abundance (to constrain dredge-up mass) and the  $^{107}\text{Pd}$  abundance (to constrain neutron fluence) in the early solar system. If, as our CBP calculations show, large amounts of  $^{26}\text{Al}$  may be produced without processing in the helium shell, then such a model loses predictive power. The role of  $^{26}\text{Al}$  in constraining the model then has to be taken up by  $^{60}\text{Fe}$  or some other nucleus.

Our work on CBP previously consisted of the single case of a  $1.5M_{\odot}$  star of solar initial composition. It is important for the AGB source hypothesis that we re-examine the consequences of CBP at other masses and metallicities. We are currently carrying out mixing calculations for several other cases, and we have found that the results are nearly universal. In particular, the possibility of producing large amounts of  $^{26}\text{Al}$  by CBP is robust, barring any physical constraints on the rate or depth of the mixing.

\*University of Perugia, Perugia, Italy, <sup>†</sup>University of Torino, Torino, Italy, <sup>‡</sup>California Institute of Technology.

<sup>1</sup>K. M. Nollett, M. Busso, and G. J. Wasserburg, *Astrophys. J.* **582**, 1036 (2003).

### c.2. Cosmic-Ray Nuclei Above the GZK Cutoff (K. M. Nollett)

It has long been predicted that the flux at the earth of cosmic rays with energy greater than about  $10^{20}$  eV (16 J) should be essentially zero. This is the so-called GZK cutoff phenomenon, and it results from protons with energy above the cutoff interacting with photons of the cosmic microwave background to produce pions. Each photopion carries off 15% or more of the proton's energy, so that it quickly falls below the cutoff. On the order of 20 air shower events with inferred energies

above the GZK cutoff have nonetheless been observed, prompting a great deal of theoretical speculation as to their source. If the extragalactic cosmic rays producing these events are not protons but are instead larger nuclei of mass  $A$ , the cutoff due to pion production shifts to an energy larger by a factor of  $A$  than the cutoff for protons. However, these nuclei will also interact with the photons from the microwave and far-infrared backgrounds by photonuclear processes that remove

nucleons from them. Previous estimates have found that as a result, their energy spectrum will also be cut off in the neighborhood of  $10^{20}$  eV. The prediction of this cutoff is not as robust as that for protons, and its severity depends on details of the (poorly-constrained) photon density in the extragalactic far-infrared background and of photonuclear cross sections.

I have developed an independent Monte Carlo code to follow the intergalactic propagation of cosmic-ray nuclei as they interact with background photons. My immediate goal is to replace the crude approximations to the photonuclear cross sections that have been used in the past. Previous calculations by other authors have all assumed that all of the photonuclear strength is concentrated in a single giant-dipole peak of Gaussian shape plus a flat response at higher photon energies. The existence of thresholds and of more complicated strength functions was neglected, even where they were prominent features of the laboratory data. Initially, I will use cross sections directly from the IAEA database

of photonuclear cross sections. At present, the transport code has been tested to reproduce old results and optimized for the speed that will be necessary for the incorporation of more complicated cross sections. The next task is to incorporate realistic photonuclear cross sections. The crucial energy range in the nuclear rest frame is from threshold to just above the giant dipole resonance.

The form of the code is completely general, so it can also be applied to the GZK problem. It could also be applied to closely-related mechanisms for producing astrophysical neutrino fluxes that will be observed in experiments like AMANDA. The pions whose decays produce the neutrinos in these mechanisms are generated by protons interacting with photons, either in the course of the GZK process, or near active galactic nuclei, or in gamma-ray bursts. This will provide a good opportunity to apply local expertise in hadronic physics to these processes.

### c.3. RIA and Astrophysics (C. D. Roberts and J. W. Truran\*)

We hosted a Theory Institute that combined expertise at Argonne National Laboratory, in the *ab initio* calculation of weak transitions and radiative capture reactions that are important in understanding the primordial composition of galaxies and in dense nucleon matter calculations relevant to neutron stars, with that in the Department of Astronomy and Astrophysics at the University of Chicago, in identifying the astrophysical sites and production time-scales of heavy element synthesis and in the analysis of neutron star observations. The Institute focused on identifying the most important theoretical problems that nuclear physicists can address in order to expedite our understanding of the synthesis of heavy elements. It stimulated interactions between Theory in PHY and the Department of Astronomy and Astrophysics at the University of Chicago. Funding was provided by the Argonne Theory Institute.

In detail, our Program supported the "Theory Symposium on Rare Isotope Accelerator Science" (April 28 - May 2, 2003), which brought experts on nuclear physics and astrophysics to the Division for a series of addresses and a laboratory-wide colloquium. Theorists and experimentalists from the Division, and the University of Chicago participated actively. The discussion centered on the efforts that must be made in tackling the uncertainties in our understanding of crucial astrophysical phenomena, such as the reliability of type-I supernovae as "standard candles" to measure the scale of the universe; and the sites of *r*-process

element production, both type-II supernovae and colliding neutron stars. A particular focus was an exploration of the potential of the experimental program at the proposed rare isotope accelerator to extract information relevant to these questions; e.g., the measurement of quantitatively reliable weak interaction and alpha-capture rates for proton rich isotopes, which are important for arriving at an understanding of type-I supernovae peak brightness.

It also supported the "Nuclear Quantum Monte Carlo Get Together," which brought practitioners of nuclear quantum Monte Carlo methods to the Division during August to discuss recent progress and coordinate new lines of research. Among the projects discussed were: a benchmark calculation of  $^{12}\text{C}$ ; calculations of electroweak transitions in light nuclei; and calculations of scattering processes. The Get Together proceeded via a series of informal seminars and working group meetings, which concentrated on technical aspects of existing projects, and on identifying means for their improvement and extension.

The final activity was a workshop on the "Surface Compositions of Accreting Neutron Stars" (September 12-13, 2003). It began with a laboratory-wide colloquium and brought a panel of experts, drawn from within the USA and abroad, to the Physics Division for a two-day focus on explosive H-He burning (the *rp*-process) on accreting neutron stars, which yields "breakout" from the CNO cycles and the subsequent

production of proton-rich nuclei through masses  $A \sim 100$ . Detailed multizone models for such events were canvassed, along with their implications for X-ray burst

light curves, the composition of the ash, and the evolution of neutron star surfaces.

---

\*Argonne National Laboratory and University of Chicago.

## D. NUCLEAR STRUCTURE AND HEAVY-ION REACTIONS

This research focuses on nuclear structure in unusual regimes: nuclei far from stability, and superdeformed nuclei at high spin. We also study heavy-ion reactions near the Coulomb barrier. Much of this work is closely tied to experiments performed at ATLAS and at radioactive beam facilities.

Our studies of heavy-ion reactions include coupled-channels calculations of fusion cross sections at energies near the Coulomb barrier. The calculated cross sections are usually quite sensitive to the structure and the radii of the reacting nuclei. This feature was exploited in an analysis of the fusion data that have been obtained for a series of germanium isotopes. Thus an irregular behavior in the radii of the germanium isotopes was identified, and it was possible from the energy dependence of the cross sections to see the difference between spherical and deformed isotopes.

We have applied our coupled-channels technique in an effort to understand what causes the suppression of heavy-ion fusion cross sections at extreme subbarrier energies. Such a suppression has been observed at ATLAS for several heavy-ion systems. We have, in particular, studied the sensitivity to the parametrization of the ion-ion potential at short distances between the reacting nuclei. Although the suppression is expected to be an entrance channel effect, and not a compound nuclear effect, it has so far not been possible to explain the data at the lowest energies.

Our studies of the proton decay from nuclei beyond the proton drip-line are based on a coupled-channels description, with a proton interacting with a deformed core nucleus. We have extended our description to include triaxial shapes of the core, in order to see how they can influence the proton decay. We find that the branching ratio of the decay to the lowest  $2^+$  state of the daughter nucleus is quite sensitive to triaxiality. We have applied the description to  $^{141}\text{Ho}$  and can in this particular case exclude any significant triaxiality.

As part of our continued interest in determining the rate of the radiative proton capture on  $^7\text{Be}$  at low energies, which is relevant to the production of  $^8\text{B}$  in the sun, we have studied the  $^7\text{Li}(n, \gamma)^8\text{Li}$  reaction and assumed charge symmetry to put constraints on the  $^7\text{Be}(p, \gamma)^8\text{B}$  reaction.

We are continuing the development of a program for calculating many-body variational wave functions that puts pairing and particle-hole two-body interactions on an equal footing. The complexity of the wave functions depends only on the number of levels included in the valence space. In these wave functions, we conserve particle number and parity strictly; projecting states of good particle number and parity before carrying out the variational calculations. We have extended the program to improve the treatment of neutron-proton pairing and have applied it to explain several features of nuclides near the  $N=Z$  line. We have also improved the procedure for optimizing our variational wavefunctions.

Our treatment of neutron-proton pairing explains many features of nuclear structure seen near the  $N = Z$  line. Our many-body treatment includes n-p pairing, as well as like particle pairing, with full projection of neutron and proton particle number before doing a variational calculation.

We also found that there is a new quantum number that holds exactly for collective states, *i.e.*, those states in which no levels are blocked. This new quantum number (Q) is the number parity of the  $T = 0$  n-p pairs. These wavefunctions explain the Wigner energy anomaly in a simple way. These wavefunctions also explain why the  $T = 0$   $1^+$  state is highly excited in  $N = Z$  even-even nuclei and very close to ground in  $N = Z$  odd-odd nuclei. Our approach predicts an asymmetry in the excitation energy of particle and hole states for nuclei in which the number of neutrons differs from the number of protons by one.

The study of low-lying states in odd-mass nuclides provides a good test of the parametrizations of single particle models. Vibrational admixtures are usually small for these states. Seven single-particle states have been identified in  $^{247}\text{Cm}$ , so this nuclide provides a particularly good test of single particle potentials. We have used a density-dependent pairing interaction to calculate pairing effects. When pairing effects are extracted from the observed levels in  $^{247}\text{Cm}$ , the orderings and spacings of levels are in good agreement with the levels obtained from our parametrization of a deformed Woods-Saxon potential.

### d.1. Coupled-Channels Calculations of Heavy-Ion Fusion at Extreme Subbarrier Energies (H. Esbensen and C. L. Jiang)

The energy dependence of heavy-ion fusion cross sections at extreme subbarrier energies was previously expected to be rather featureless, once the enhancement due to coupled-channels effects had saturated. It was therefore a great surprise for us to see that the measured cross sections for several heavy-ion systems showed an unexpected steep falloff at extreme subbarrier energies.<sup>1</sup> The steep falloff sets in typically at 20-30 MeV above the ground state of the compound nucleus so compound nuclear effects should not play a role. The steep falloff is expected to be an entrance channel phenomenon, and we have investigated whether such a phenomenon occurs in conventional coupled-channels calculations.<sup>2</sup>

An example of a system that exhibits a steep fall off at low energies is  $^{64}\text{Ni} + ^{64}\text{Ni}$ . This is illustrated in Fig. V-11 where we show the logarithmic derivative extracted from the data and from various calculations. The logarithmic derivative is defined as

$$L(E) = \frac{1}{E\sigma_f} \frac{d}{dE} (E\sigma_f) \quad (1)$$

in terms of the fusion cross section  $\sigma_f$  and the cm energy  $E$ . The thin dashed curve shows the behavior of

the no-coupling calculation. The two curves that oscillate at low energy are from coupled-channels calculations, which employ different ion-ion potentials at short distances. The solid curve shows an attempt to optimize the fit to the data<sup>3</sup> but it is seen that the fit eventually fails at the lowest energy.

Measurements of the  $^{64}\text{Ni} + ^{64}\text{Ni}$  fusion have recently been performed at ATLAS down to even lower energies.<sup>4</sup> It turns out that the logarithmic derivative extracted from the new data keeps increasing steeply with decreasing energy. It even exceeds, at the lowest energies, the  $L(E)$  that one obtains for a constant S factor (upper curve). The steep rise of the  $L(E)$  obtained in coupled-channels calculations, on the other hand, seems always to level off at low energies. The same feature occurs in calculations for other systems so it appears that the phenomenon, which is responsible for the observed steep rise in  $L(E)$  with decreasing energy, is not contained in conventional coupled-channels calculations. It is interesting to note that measured and calculated  $L(E)$  start to depart at an energy where average angular momentum of the compound nucleus reaches a constant. This can be seen in Fig. V-12. Part of this work was presented at the conference FUSION03.<sup>5</sup>

<sup>1</sup>C. L. Jiang *et al.*, Phys. Rev. Lett. **89**, 052701 (2002).

<sup>2</sup>C. L. Jiang *et al.*, Phys. Rev. C **69**, 014604 (2004).

<sup>3</sup>D. Ackermann *et al.*, Nucl. Phys. **A609**, 91 (1996).

<sup>4</sup>C. L. Jiang *et al.*, see Experimental Section of the Annual Report, Fig. I-59.

<sup>5</sup>H. Esbensen, Proceedings of International Conference FUSION03: "From a Tunneling Nuclear Microscope to Nuclear Process in Matter," Matsushima, Mayagi, Japan, November 12-15 (2003).

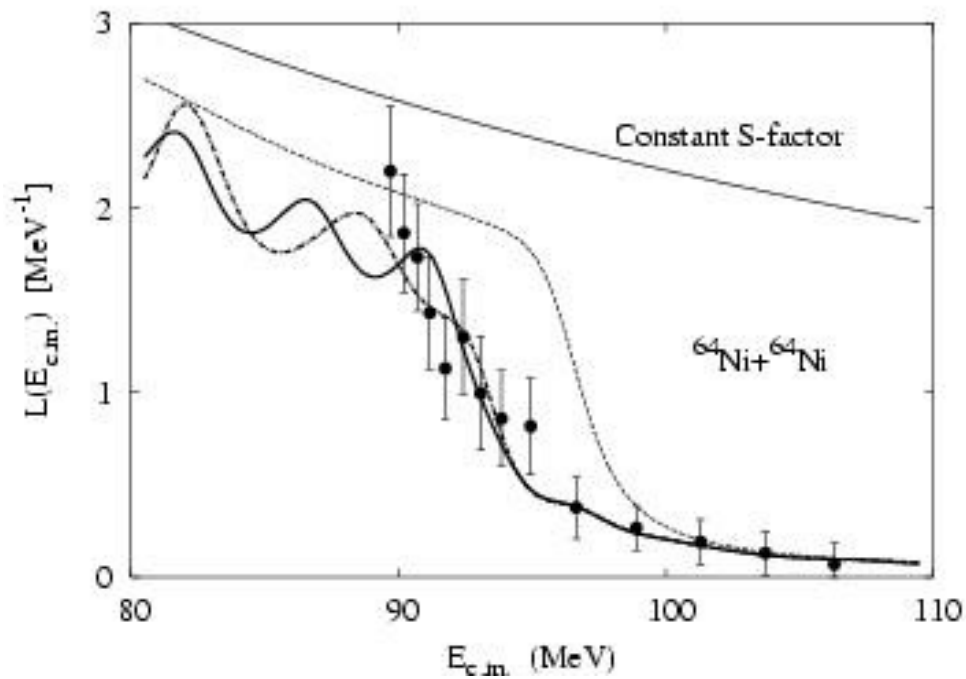


Fig. V-11. Logarithmic derivative of the fusion cross section discussed in the text. The data are from Ref. 3. The top curve is the result for constant S factor.

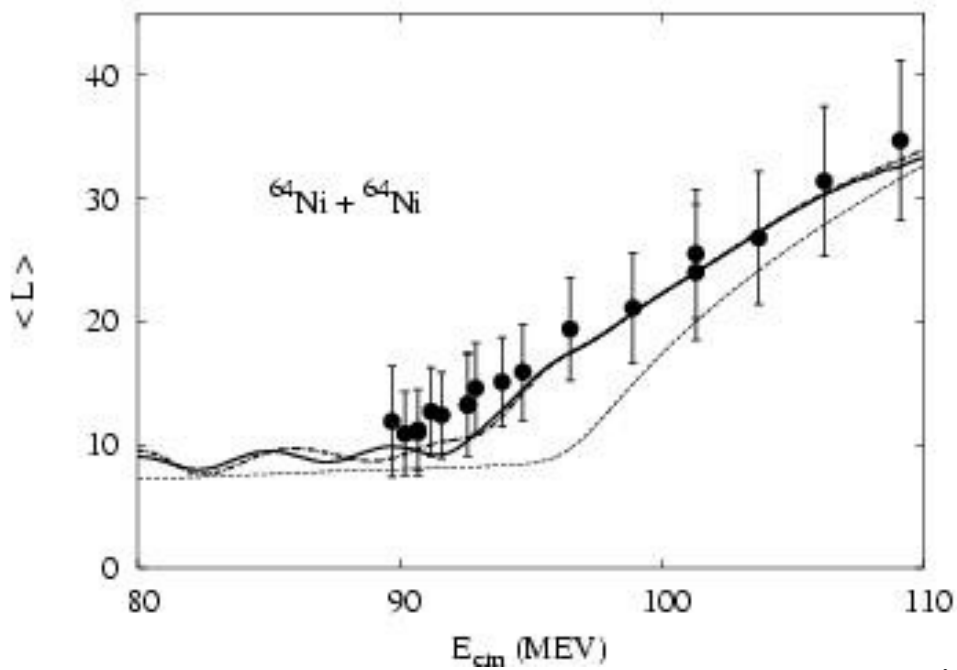


Fig. V-12. Average spin of the compound nucleus, extracted from the measured  $\gamma$ -ray multiplicity.<sup>3</sup> The curves correspond to those shown in Fig. V-11.

### d.2. Decay Rate of a Triaxially Deformed Proton Emitter (C. N. Davids and H. Esbensen)

Calculations of the decay rate for a triaxially deformed proton emitter have been performed in a particle-rotor model, based on a deformed Woods-Saxon potential. The calculations described in the 2002 Annual Report used an axially-symmetric spin-orbit interaction between the proton and the core. We have now extended these calculations by employing a fully deformed spin-orbit interaction, including an angle-dependent diffuseness. As an application, the wave function of the  $I = 7/2^-$  ground state of the deformed proton emitter  $^{141}\text{Ho}$  is obtained in the adiabatic limit, and a Green function technique is used to calculate the

total decay rate and the branching ratio to the first excited  $2^+$  state of the daughter nucleus  $^{140}\text{Dy}$  at an excitation energy of 202 keV. Figure V-13 shows the calculated value of the branching ratio for decay to the first excited  $2^+$  state vs. the triaxial angle  $\gamma$  (solid line) compared with the experimental value (shaded area).<sup>1</sup> The generic error bar on the calculated value is due to the uncertainty in the measured proton energy.<sup>2</sup> Only for values of the triaxial angle  $\gamma < 5^\circ$  is good agreement obtained for both the total decay rate and the  $2^+$  branching ratio.<sup>2</sup> This work was published.<sup>3</sup>

<sup>1</sup>C. N. Davids *et al.*, Phys. Rev. Lett. **80**, 1849 (1998).

<sup>2</sup>K. Rykaczewski *et al.*, Proceedings of International Conference on Nuclear Structure, "Mapping the Triangle," Grand Teton National Park, Wyoming, May 22-25, 2002, AIP Proceedings **638**, 149 (2002).

<sup>3</sup>C. N. Davids and H. Esbensen, Phys. Rev. C **69**, 034314 (2004).

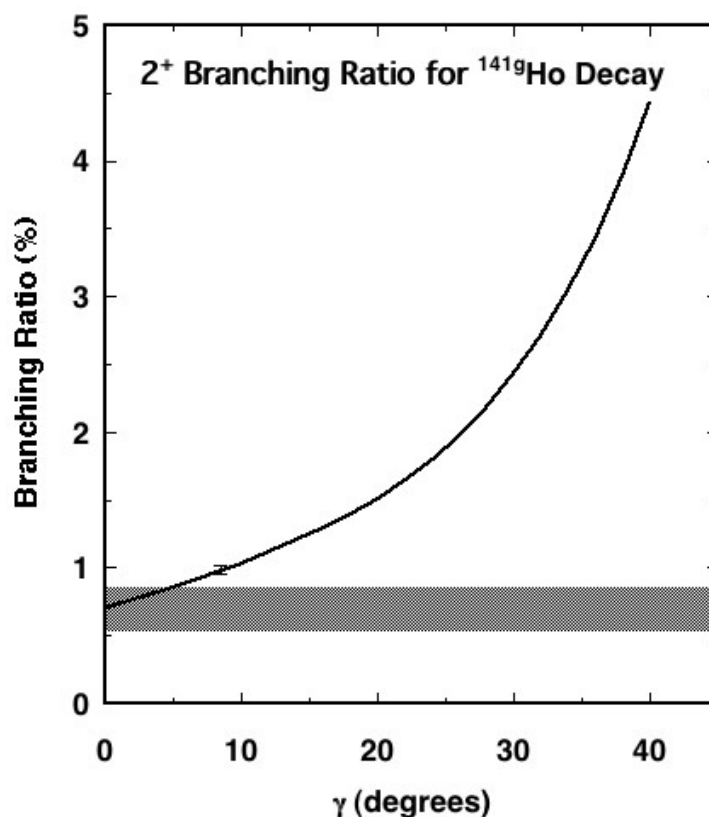


Fig. V-13. Calculated  $2^+$  branching ratio for the proton decay of  $^{141g}\text{Ho}$ , plotted as a function of the triaxial angle  $\gamma$  (solid line), and the experimental value (shaded area).

### d.3. Constraints on the ${}^7\text{Be}(p,\gamma){}^8\text{B}$ Reaction from Charge Symmetry (H. Esbensen)

The radiative proton capture rate on  ${}^7\text{Be}$  at energies relevant to the interior of the sun is usually expressed in terms of the S factor at zero relative energy,  $S_{17}(0)$ . The recommended value<sup>1</sup> back in 1998 was  $S_{17}(0) = 19 \pm \frac{4}{2}$  eV b. A large experimental effort has since gone into reducing the uncertainty on this value. The overlap between the new results is unfortunately marginal in some cases.

The analysis of measurements (radiative capture, Coulomb dissociation, transfer) are often based on a two-body model of the valence nucleon interacting with the  ${}^7\text{Be}$  core. It is therefore of interest to determine the range of values of  $S_{17}(0)$  one can obtain from such a simple model when certain constraints are imposed. In this study the experimental knowledge of the charge symmetric  ${}^7\text{Li}(n,\gamma){}^8\text{Li}$  reaction is used to put constraints on the model.

The radiative capture cross sections for the charge symmetric reactions,  ${}^7\text{Be}(p,\gamma){}^8\text{B}$  and  ${}^7\text{Li}(n,\gamma){}^8\text{Li}$ , have been calculated in a two-body model. The nuclear interaction is parametrized as a Woods-Saxon well, and the well depth is adjusted for each reaction channel so that binding energies and neutron s-wave scattering lengths are reproduced. The ground states of  ${}^8\text{B}$  and  ${}^8\text{Li}$  are described as a  $p_{3/2}$  valence nucleon coupled to the

$3/2^-$  ground state of  ${}^7\text{Be}$  and  ${}^7\text{Li}$ , respectively. The low energy radiative capture proceeds via E1 transitions from continuum s- and d-waves. The results of the calculations are expressed in terms the value of  $S_{17}(0)$  for  ${}^8\text{B}$  and the normalization factor  $N_{nc}$  that is required to reproduce the low-energy neutron capture rate on  ${}^7\text{Li}$ .

The calculations have been repeated for a wide range of the radius  $R$  and for different values of the diffuseness  $a$  of the Woods-Saxon well. The correlation between  $N_{nc}$  and  $S_{17}(0)$  which is mediated by the values of  $(R,a)$  is shown in Fig. V-14 by the dashed curves. One can interpret the factor  $N_{nc}$  as a spectroscopic factor for  ${}^8\text{Li}$ . Choosing a certain preferred value (the horizontal line shows  $N_{nc} = 0.87$ ) one can then predict the S-factor.

Assuming charge symmetry, one could also interpret  $N_{nc}$  as the spectroscopic factor for  ${}^8\text{B}$  and use it to determine the effective S factor which is given by the product  $N_{nc} \times S_{17}(0)$ . This estimate is shown by the solid curves in the figure. The predictions are seen to fall in a surprisingly narrow range around 19 eV b. This result must be taken with a grain of salt. There are several uncertainties in the model, which are currently being investigated.

<sup>1</sup>E. G. Adelberger *et al.*, Rev. Mod. Phys. **70**, 1265 (1998).

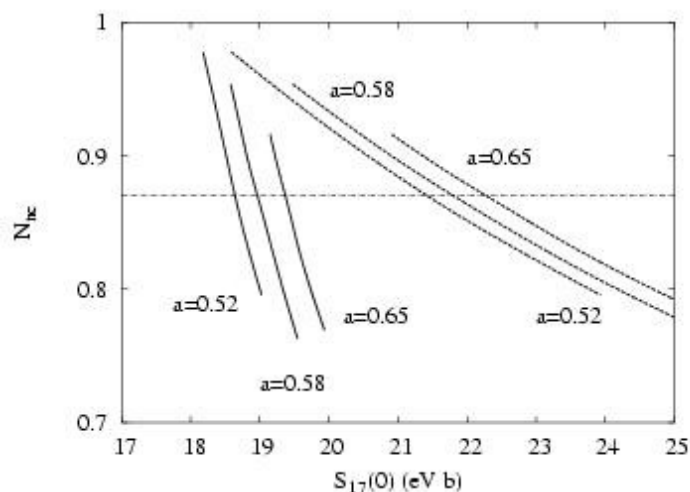


Fig. V-14. The dashed curves show the correlation between the normalization factor  $N_{nc}$  for the neutron capture on  ${}^7\text{Li}$  and the calculated S factor for  ${}^8\text{B}$ , obtained for different values of the diffuseness  $a$ . The correlation is mediated by the radius of the Woods-Saxon well. The solid curves show the correlation between  $N_{nc}$  and the product  $N_{nc} \times S_{17}(0)$ .

#### d.4. Fusion Reactions with Germanium Isotopes (H. Esbensen)

The measured cross sections<sup>1,2</sup> for the fusion of  $^{16}\text{O}$  and  $^{27}\text{Al}$  with a series of germanium isotopes have been analyzed within the coupled-channels formalism. The calculations are performed in the so-called rotating frame approximation (RFA), which makes it feasible to include many channels in the calculations, as for example, two-phonon and mutual excitations of the low-lying surface modes. It is also shown how one can handle (in the RFA) the excitation of an odd nucleus, like  $^{27}\text{Al}$ , with a non-zero ground state spin.

The calculations include the elastic channel, the excitation of low-lying  $2^+$  and  $3^-$  states in projectile and target, mutual excitations of these, and also the two-phonon quadrupole excitation in the germanium isotopes. It is demonstrated that it is not possible to achieve a good fit to the data when the calculations are based on couplings that are linear in the deformation amplitudes. It is necessary to include at least quadratic nuclear couplings in order to get a good fit. This is

illustrated for the  $^{16}\text{O}$  and  $^{27}\text{Al}$  fusion with  $^{74}\text{Ge}$  in Figs. V-15 and V-16. The dashed curves were in both cases obtained without any couplings. The dotted-dashed curves are based on linear couplings. The solid curves are based on linear and quadratic couplings.

Calculated fusion cross sections are quite sensitive to the structure and the radii of the reacting nuclei. One can exploit this feature in the analysis of the fusion data for a series of isotopes like germanium. From the analysis it is concluded that the radius of  $^{74}\text{Ge}$  must be about 0.1 fm smaller than predicted by a smooth interpolation between the radii of the other germanium isotopes. The smaller radius may reflect the shell closure for  $N = 40$  neutrons. It is also found that  $^{74}\text{Ge}$  must be near spherical, instead of having a large quadrupole deformation as previously thought. These conclusions are supported both by the analysis of the  $^{16}\text{O}$  and the  $^{27}\text{Al}$  induced reactions. This work was published.<sup>3</sup>

<sup>1</sup>E. F. Aguilera *et al.*, Phys. Rev. C **52**, 3103 (1995).

<sup>2</sup>E. F. Aguilera *et al.*, Phys. Rev. C **41**, 910 (1990).

<sup>3</sup>H. Esbensen, Phys. Rev. C **68**, 034604 (2003).

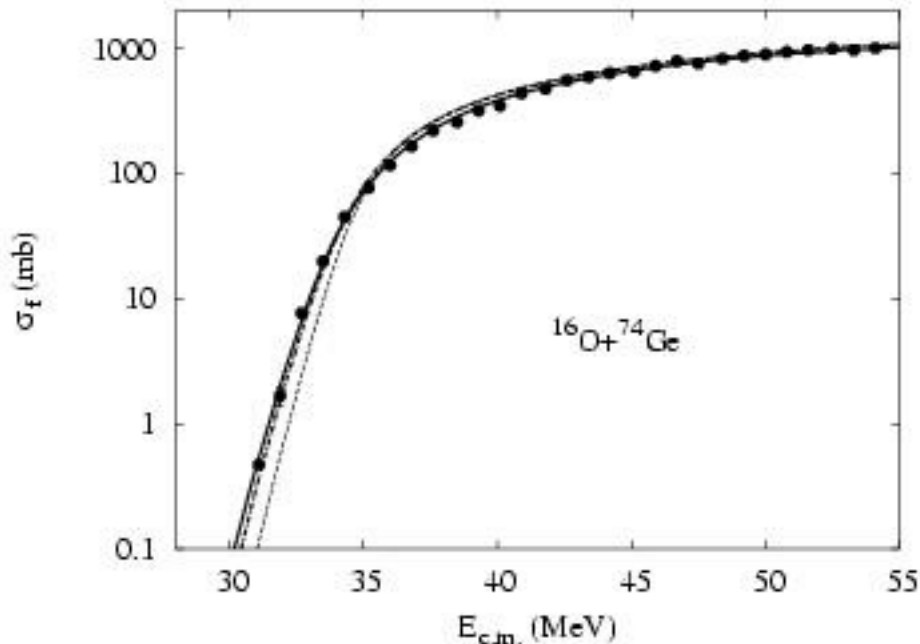


Fig. V-15. Fusion cross sections for  $^{16}\text{O}+^{74}\text{Ge}$ .<sup>1</sup>

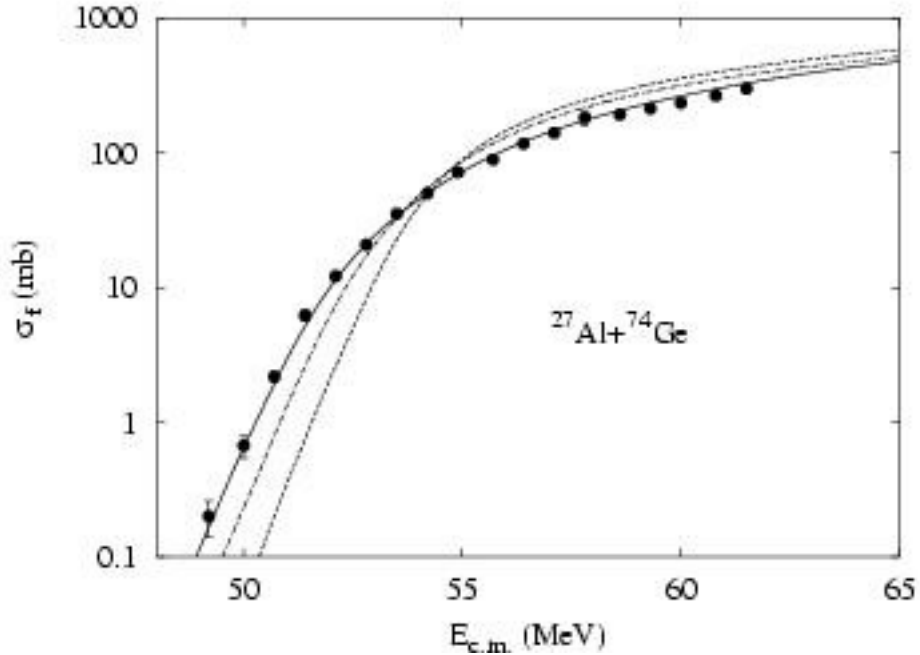


Fig. V.16. Fusion of  $^{27}\text{Al} + ^{74}\text{Ge}$ .<sup>2</sup>

#### d.5. Mean Field and Many Body Wave Functions (R. R. Chasman)

We are continuing the development of a program for calculating many-body variational wave functions that puts pairing and particle-hole two-body interactions on an equal footing. The complexity of the wave functions depends only on the number of levels included in the valence space. In these wave functions, we conserve particle number and parity strictly, projecting states of good particle number and parity before carrying out the variational calculations. We have extended the program to improve the treatment of neutron-proton pairing and have applied it to explain several features of nuclides near the  $N = Z$  line. We have also improved the procedure for optimizing our variational wavefunctions.

By using residual interaction strengths (*e.g.*, the quadrupole interaction strength or pairing interaction strength) as generator coordinates, one gets many

different wave functions, each having a different expectation value for the relevant interaction mode. Such wave functions are particularly useful when one is dealing with a situation in which a configuration interaction treatment is needed. Because the same basis states are used in the construction of all the many-body wave functions, it is possible to easily calculate overlaps and interaction matrix elements for the many-body wave functions obtained from different values of the generator coordinates (which are not in general orthogonal). The valence space can contain a very large number of single-particle basis states, when there are constants of motion that can be used to break the levels up into subgroups. To increase the manageable size of the valence space, we have parallelized our code to run on the SP computer system, and we are modifying the code to deal with octupole correlations in heavy nuclei.

### d.6. Wave Function Optimization (R. R. Chasman)

We have improved the procedure for optimizing our variational wavefunctions. This is an ongoing effort. There is no general solution to this problem and there is always a danger of becoming trapped in a local minimum rather than the global minimum. The problem is particularly serious when there are many amplitudes in the variational wavefunction. One can often get around the fact that a single variational function is not optimal by taking linear combinations of wavefunctions and doing a configuration interaction calculation. However, it is preferable to get an optimal many-body variational wavefunction and then use it in a configuration interaction calculation. The fewer the number of wavefunctions that are needed in a configuration interaction diagonalization, the easier it is to get some insight into the physics.

We have found that our variational wavefunctions can be improved in a systematic way by removing all phase and magnitude information from a single subgroup in the many-body wavefunction, *i.e.*, we set all variational amplitudes in the subgroup equal to each other and then use this modified wavefunction as the starting point for our variational minimization procedure. This is done for all of the subgroups in turn. If the energy is not improved, when a given subgroup is modified in this way, we take the prior wavefunction as the starting point for modifying the next subgroup. We have applied this procedure to many different starting wavefunctions for the same nucleus. The starting wavefunctions differ by several MeV in energy. Using this procedure, we end up with energies that differ by a few hundred keV. We continue to explore optimization procedures for variational wavefunctions.

### d.7. Neutron-Proton Pairing (R. R. Chasman)

We have developed<sup>1-3</sup> a treatment of neutron-proton pairing that explains many features of nuclear structure seen near the  $N = Z$  line. Our many-body treatment includes n-p pairing, as well as like particle pairing, with full projection of neutron and proton particle number before doing a variational calculation. We also found that there is a new quantum number that holds exactly for collective states, *i.e.*, those states in which no levels are blocked. This new quantum number ( $Q$ ) is the number parity of the  $T = 0$  n-p pairs. Fixing the number parity of one n-p mode fixes the other, because we conserve proton number and neutron number exactly. This number parity is closely related to the isospin quantum number. These collective states are the ground states for  $N = Z$  nuclides. We project  $Q$  before doing a variational calculation. By doing calculations that conserve  $Q$ , we find a remarkable multiplicity of degenerate levels in odd-odd nuclides, with  $N = Z (\pm 2m)$ . Such multiplets are at or near ground for  $m = 1$  or  $2$ . The form of our variational wave function includes an explicit amplitude for "alpha like" correlations in each level as well as the usual amplitudes for n-n, p-p and n-p pairs. We have added terms to the n-p pairing interaction that allow pairs of particles in the same orbitals, giving states with maximum angular momentum. Because of the exclusion principle, these must be n-p pairs and  $T = 0$ .

In odd-odd  $N = Z$  nuclei, the ground state is a degenerate doublet, consisting of a  $Q = 0$  and  $Q = 1$  state, when the  $T = 0$  and  $T = 1$  pairing strengths are

equal. The splitting of this ground state doublet affords some information about the relative strengths of the  $T = 0$  and  $T = 1$  pairing strengths. In even even nuclei, there is a large splitting between the  $0^+ T = 1$  ground state and the  $1^+ T = 0$  excited state. Our model explains this feature in a transparent way. Most of the excitation energy is due to the breaking of a quartet and the single particle excitation energy involved in making a  $T = 0$  pair. In the odd-odd  $N = Z$  nuclei case, neither of these effects applies for the  $T = 0$  state. In Fig. V-17, we display the excitation energy of the  $T = 1$  state in both odd-odd and even-even  $N = Z$  nuclides. The excitation energy is shown as a function of  $T = 0$  pairing strength, while the  $T = 1$  pairing strength is held constant.

The Wigner energy is the extra binding energy of  $N = Z$  even-even nuclei relative to neighboring nuclei. Our approach explains the magnitude of the Wigner energy very well. It is due to the extra pairing energy involved in creating a quartet of nucleons in the same orbital.

In addition to the collective states discussed above, there are configurations in which one or more levels are blocked. These configurations constitute the ground states of all odd-mass nuclides and are likely to be the ground state or close in energy to the ground state of odd-odd nuclei with a neutron excess. For these blocked levels, the amplitudes are complex. We extended our treatment of n-p pairing to include configurations with blocked levels. Our approach explains the experimental observation<sup>4</sup> that the level

density is quite low for  $N = Z$  odd-odd nuclei and rises substantially in nuclei with two more neutrons. In Figs. V-18 and V-19, we show the low-lying states for an odd-odd  $N = Z$  system with equally spaced levels and the low-lying states in a system with two more neutrons. In the  $N = Z + 2$  system, both blocked configurations and unblocked configurations are near ground. In the  $N = Z$  system, the blocked configurations are highly excited.

Our approach also predicts an asymmetry between particle and hole states in odd mass nuclides near the  $N = Z$  line. In odd mass nuclides that have one nucleon in addition to an even-even  $N = Z$  core, our model suggests that the first excited state will be a particle state on the average. In odd mass nuclides with one nucleon removed from an even-even  $N = Z$  core, the first excited state is expected to be a hole state.

<sup>1</sup>R. R. Chasman, Phys. Lett. **B524**, 81 (2002).

<sup>2</sup>R. R. Chasman, Phys. Lett. **B553**, 204 (2003).

<sup>3</sup>R. R. Chasman, Phys. Lett. **B577**, 47 (2003).

<sup>4</sup>D. G. Jenkins *et al.*, Phys. Rev. C **65**, 064307 (2002).

### Q-splitting in $N=Z$ Nuclei

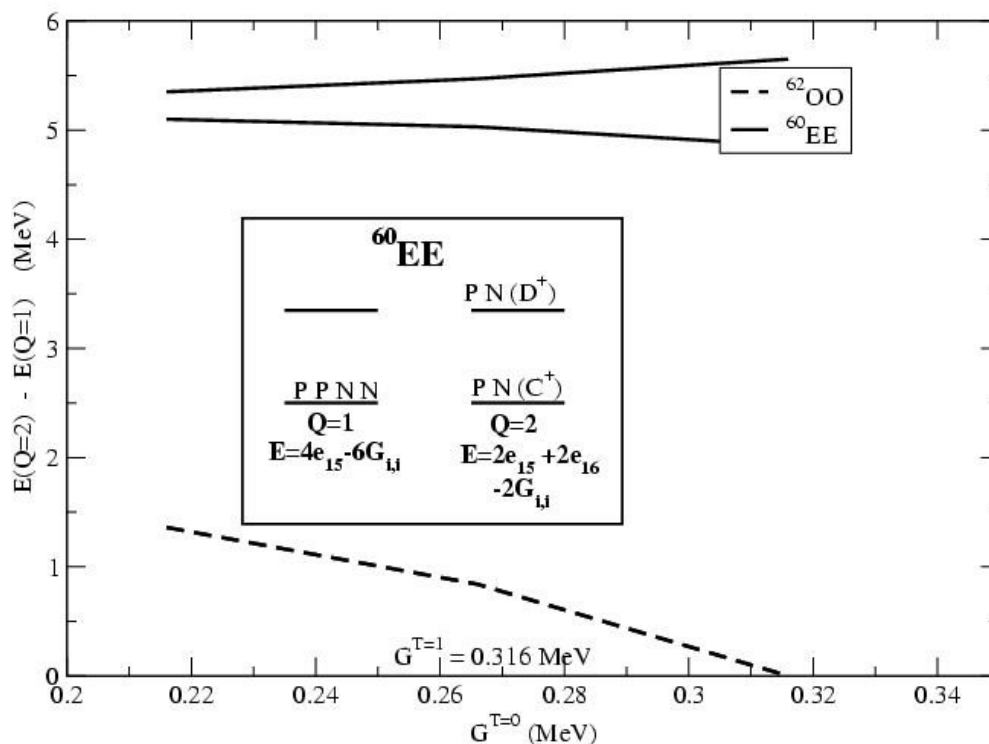


Fig. V-17. Excitation Energy of  $Q = 2$  States in  $N = Z$  Nuclei. In this figure, and the following two figures, levels and excitation energies are shown for idealized nuclei, having a constant energy difference between single particle levels and having constant pairing matrix energy.  $^{60}\text{EE}$  designates the idealized even-even nucleus having 30 protons and 30 neutrons.  $^{62}\text{OO}$  designates the idealized odd-odd nucleus with 31 protons and 31 neutrons.  $^{64}\text{OO}$  designates the idealized nucleus with 31 protons and 33 neutrons. The excitation energy is plotted as a function of  $G^{T=0}$  for  $G^{T=1}$  fixed at 0.316 MeV. The solid lines show the excitation energy of the  $Q = 2$  states in  $^{60}\text{EE}$ . The dashed line shows the excitation energy of the lowest  $Q = 2$  state in  $^{62}\text{OO}$ . The results are obtained from a configuration interaction calculation. In the box, we show the Slater determinant approximation for the distribution of protons and neutrons for  $Q = 1$  and  $Q = 2$  in the even-even case. The letter  $P(N)$  above a line indicates a proton (neutron) in that level. The two levels shown are levels 15 and 16. All levels below level 15 are filled in this order. The energy expressions are the Slater energies, which consist of single particle energies plus diagonal pairing energies.

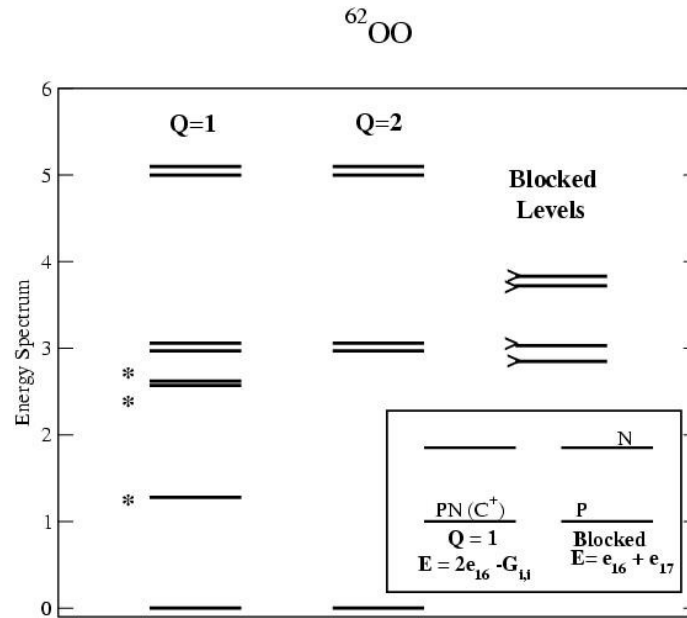


Fig V-18. Excitation Energies of  $Q = 1$ ,  $Q = 2$  and Blocked States in  $^{62}\text{OO}$ .  $G^{T=0}$  and  $G^{T=1}$  have the value of 0.316 MeV. The arrowhead on the left of all blocked levels indicates an additional factor of two in the number of levels coming from the two values of  $\Omega$  with  $\Omega = |\Omega_1 \pm \Omega_2|$ . The  $\Omega$ -blocked levels in the  $Q = 1$  column are marked with an asterisk. In the box, the Slater determinant occupations of levels 16 and 17 are shown, for the lowest  $Q = 1$  state and the lowest blocked state. The Slater energies are also given.

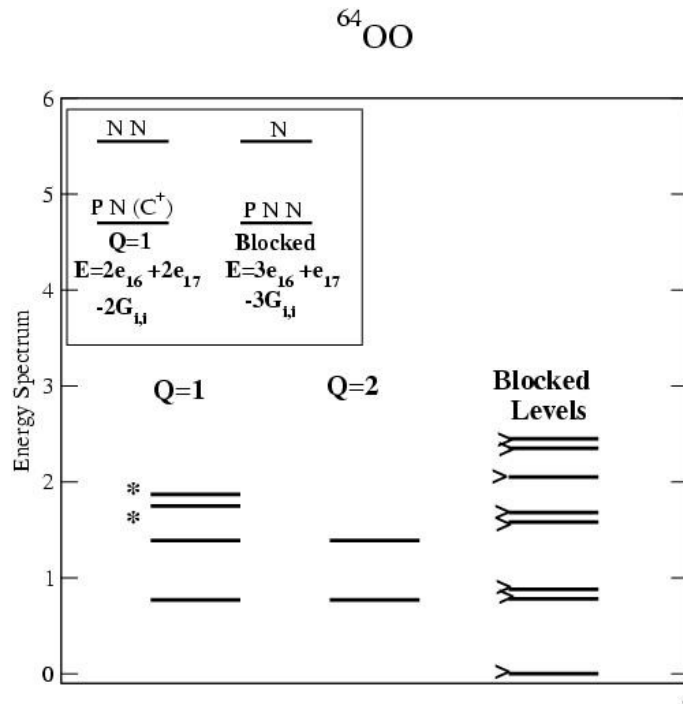


Fig. V-19. Excitation Energies of  $Q = 1$ ,  $Q = 2$  and Blocked States in  $^{64}\text{OO}$ . Off-diagonal  $G^{T=0}$  and  $G^{T=1}$  matrix elements have the value of 0.316 MeV. The arrowhead on the left of all blocked levels indicates an additional factor of two in the number of levels coming from the two values of  $\Omega$  with  $\Omega = |\Omega_1 \pm \Omega_2|$ . The  $\Omega$ -blocked levels in the  $Q = 1$  column are marked with an asterisk. In the box, the Slater determinant occupations of levels 16 and 17 are shown, for the lowest  $Q = 1$  state and the lowest blocked state. The Slater energies are also given.

**d.8. Energy Levels of  $^{247}\text{Cm}$**  (I. Ahmad, R. R. Chasman, J. P. Greene, F. Kondev, E. F. Moore, E. Browne,\* C. E. Porter,† and L. K. Felke‡)

The study of low-lying states in odd-mass nuclides provides a good test of the parametrizations of single particle models. Vibrational admixtures are usually small for these states. Seven single-particle states have been identified<sup>1</sup> in  $^{247}\text{Cm}$ , so this nuclide provides a particularly good test of single particle potentials.

When pairing effects are extracted from the observed levels in  $^{247}\text{Cm}$ , using a density-dependent pairing interaction, the orderings and spacings of levels are in good agreement with the levels obtained from our parametrization of a deformed Woods-Saxon potential.

\*Lawrence Berkeley National Laboratory, †Oak Ridge National Laboratory.

<sup>1</sup>I. Ahmad *et al.*, Phys. Rev. C **68**, 044306 (2003).

**d.9. Octupole Correlations in Light Actinides** (R. R. Chasman)

The difficulty in dealing with octupole correlations in the light actinides is that the effects are not sufficiently large to give rise to a well defined deformation. A many-body wave function is needed to deal effectively with these correlations. We started to apply our many-body approach to a re-examination of this region. In our early work, which was the first to predict parity doublets in the odd-mass nuclides of this region, we were limited to subgroups of at most five Nilsson orbitals. Advances in our code and the use of parallel

processing make it feasible to deal with subgroups consisting of as many as eight Nilsson orbitals. One application of this calculation will be a study of the structure of the  $\frac{1}{2}^{\pm}$  parity doublet in  $^{225}\text{Ra}$ , that is being studied to put new upper limits on the dipole moment of the neutron. The new optimization procedure discussed above will be quite helpful in the calculation of octupole correlations.

**d.10. Self-Consistent Beyond-Mean-Field Calculations in Exotic Heavy Nuclei** (T. Duguet, M. Bender,\* P.-H. Heenen,† and P. Bonche‡)

We extended the Goldstone-Brueckner perturbation theory to motivate methods beyond the mean-field such as the Generator Coordinate Method and the Projected Mean-field Method. We derived the effective interaction removing the hard-core of the bare nucleon-nucleon force accordingly. Simplifying this effective vertex, we extended the applicability of the Skyrme interaction to configuration mixing calculations.

performing a configuration mixing of angular-momentum and particle-number projected self-consistent mean-field states. This study supported the interpretation of spectra made on the grounds of more schematic models in terms of coexisting spherical, oblate, prolate and superdeformed prolate structures. Theoretical spectra and transition probabilities (E0 and E2) are in relatively good agreement with experimental data. We predicted the presence of superdeformed bands at low excitation energy in the most neutron-deficient isotopes.

We studied the low-lying collective excitation spectra of the neutron-deficient lead isotopes  $^{182}\text{Pb}$ - $^{194}\text{Pb}$  by

\*M. Bender, Institute of Nuclear Theory, University of Washington, †P.-H. Heenen Universite Libre de Bruxelles, Belgium, ‡P. Bonche, Commissariat a L'Energie Atomique, Saclay, France.

**d.11. A New Microscopic Pairing Force for Self-Consistent Mean-Field Calculations (T. Duguet)**

We derived a microscopic finite-range effective pairing force from the bare nucleon-nucleon interaction. It reproduces exactly the pairing provided in infinite matter by the AV18  $NN$  interaction. By going from the bare to a well-defined effective force explicitly, we disentangled the effects of the range and of the density dependence of the effective pairing interaction. In particular, the relative success of existing

phenomenological finite-range/density-independent and zero-range/density-dependent forces could be explained on a more fundamental basis. The interaction was made simple enough to be used in self-consistent mean-field calculations of finite nuclei. Three-dimensional HFB calculations using this new microscopic interaction are now underway.

## E. ATOMIC THEORY AND FUNDAMENTAL QUANTUM MECHANICS

In addition to research on hadronic and nuclear physics, and nuclear astrophysics, we also conduct research in atomic physics, neutron physics, and quantum computing.

Work in atomic physics includes the studies of interactions of electrons or high-energy photons with matter, in support of experiments performed at Argonne's Advanced Photon Source (APS). Theoretical studies are being conducted on the physics of the photoeffect and Compton scattering by bound electrons, focusing on topics selected in view of basic importance, timeliness, and potential in applications. Data on crystalline silicon for the interactions of photons over the entire spectral range were comprehensively analyzed with the use of dispersion relations and sum rules, and results are being prepared for publication. The analysis of dispersion relations was also found to be a powerful tool for interpreting data on refraction from various glasses used in optical devices.

Theoretical work in support of a new experiment to measure the neutron electric-dipole moment continues. A proof-of-principle experiment to measure the neutron magnetic-dipole moment in the same way has been approved for the Missouri University Research Reactor and should be carried out in FY 2004. In addition, work continues to extend the spin-statistics theorem in nonrelativistic quantum mechanics to particles with non-zero spins. Recent progress has been clarification of issues involving spatial rotations of identical particles.

Work continued toward the development of a coherent theory of physics and mathematics. The studies consisted of emphasizing both the physical nature of language and some aspects of the theory-experiment connection. We proposed to tighten the theory experiment connection by replacing the complex numbers on which physical theories are based, by length  $n$  string numbers, which have the characteristics of measurement outcomes. Consequences of this replacement, including an exploration of the limit  $n \rightarrow \infty$ , are being studied.

### e.1. Interactions of Photons with Matter (M. Inokuti and D. Y. Smith\*)

In support of experiments in atomic and condensed-matter physics with the use of synchrotron radiation, theoretical studies are being conducted on the physics of photo-absorption and Compton scattering, focusing on topics selected in view of basic importance, timeliness, and potential applications.

One theme of long-term studies has been the use of

dispersion relations and sum rules for indices of response of matter over the entire range of photon energies. A comprehensive analysis of optical data on silicon is nearly complete and work on graphite has begun. A novel method for characterizing the refractive index of a substance in a region of near transparency was formulated and applied to silicate glasses.<sup>1</sup>

---

\*University of Vermont.

<sup>1</sup>D. Y. Smith, M. Inokuti, and W. Karstens, *Radiat. Effects Defects Solids* **157**, 823 (2002).

### e.2. Interactions of Charged Particles with Matter (M. Inokuti)

Stopping power, the total yield of ionization, and its statistical fluctuations are examples of quantities describing the penetration of charged particles through matter and are important to applications such as the detection of particles and the analysis of their charges and kinetic energies. The understanding of those quantities in terms of individual collisions and associated cross sections remains a major challenge and is the goal of our continuing effort. Current work is the evaluation of the mean excitation energies, namely, the  $I$  values, in the Bethe stopping-power formula from the

oscillator-strength spectra for nine atoms and 23 molecules that are given by Berkowitz.<sup>1</sup>

The cross section for triple ionization of the lithium atom by electron impact, recently measured by Argonne colleagues, was interpreted.<sup>2</sup>

Extensive work for the International Commission on Radiation Units and Measurements (ICRU) continues on the editing of its reports and on physical data such as stopping powers and various interaction cross sections.

---

<sup>1</sup>J. Berkowitz, *Atomic and Molecular Photoabsorption. Absolute Total Cross Sections* (Academic Press 2002).

<sup>2</sup>M.-T. Huang, W. W. Wong, M. Inokuti, S. H. Southworth, and L. Young, *Phys. Rev. Lett.* **90**, 163201 (2003).

### e.3. Spin and Statistics in Nonrelativistic Quantum Mechanics (M. Peshkin)

I earlier proved that identical spin-zero particles with no internal degrees of freedom must be bosons. That proof used standard assumptions of nonrelativistic quantum mechanics plus the assumption that the wave function must depend upon the unordered pairs  $\{\mathbf{r}_1, \mathbf{r}_2\}$ , for which  $\{\mathbf{r}_2, \mathbf{r}_1\}$  is the same point in the configuration space as is  $\{\mathbf{r}_1, \mathbf{r}_2\}$ . That added assumption, which was introduced by Leinaas and Myrheim and developed by Berry and Robbins, is motivated by the idea that the wave function for indistinguishable particles should not depend upon fictitious particle labels but only upon the pairs of points they occupy. It does not immediately lead to boson behavior because the symmetry of the usual wave function under exchange of  $\mathbf{r}_1$  and  $\mathbf{r}_2$  has no useful counterpart in the space of the unordered pairs. That the particles must be bosons was proved by making use of the behavior of the wave functions under rotation and of smoothness requirements on wave

functions imposed by the second derivatives in the Hamiltonian.

That work has now been published and it has evoked questions from others along two lines. One, which has been published as a Comment, questions the relation of the theory to standard quantum mechanics. I have now shown in a published reply that there is in fact no difference between this theory and standard quantum mechanics except for the intended difference that here the boson statistics are justified within the theory rather than imposed externally. In that sense the present work justifies the usual procedure of labeling coordinates by the non-existent particle labels and then imposing symmetry of the wave function under particle exchange. The second question deals with the behavior of identical-particle wave functions under rotation. I have now obviated that question by giving a new proof

which does not involve the behavior of wave functions under rotation. That work is being prepared for publication.

Ongoing research is attempting to treat particles with non-zero spins in a similar way.

#### **e.4. Towards a Coherent Theory of Mathematics and Physics: The Theory Experiment Connection (P. Benioff)**

Work was begun on a study of some aspects of the connection between theory and experiment as an important part of a coherent theory of physics and mathematics. The work, which is based on earlier papers,<sup>1</sup> noted the existence of a theory hierarchy as a component of comparing theory predictions with experimental results. The validity of the theories on which the proper functioning of experimental equipment is based must be known prior to that of the theory being tested by the experiment in question. The need for computers in making the theory experiment comparison was noted. The viewpoint here, which is different from the usual one, is that computers serve to interpolate or translate names of real numbers as equations into finite strings of digits which correspond to experiment outputs. The main part of the work concerns tightening the theory experiment connection

by replacing the complex numbers  $C$  on which physical theories are based by the set  $C_n$  of pairs of length  $n$  strings of digits in some basis. The basic idea is that one requires that any  $C_n$  based theory  $Th_n$  be supported by all experiments appropriate for the numbers in  $C_n$  and then takes the limit  $n$  to infinity to recover  $C$  based physics. Much of the work concerned developing the properties of space and time based on the numbers in  $R_n$ . These included the discreteness of the space, the presence of space singularities and the scale invariance of space. Also the flexibility of  $R_n$  space based on its dependence on two integer parameters,  $n$  and  $e$ , showed that translational type transformations are a combination of exponential jumps and usual lattice type translations with the balance between the two types regulated by  $n$ .

<sup>1</sup>P. Benioff, Foundations of Physics **32**, 989-1029 (2002).

<sup>2</sup>P. Benioff, Quantum Information Processing **1**, 495-509 (2002).

#### **e.5. The Representation of Real and Complex Numbers in Quantum Mechanics (P. Benioff)**

Earlier work on the representation of rational numbers,<sup>1</sup> integers,<sup>1</sup> and natural numbers<sup>2</sup> in quantum mechanics is being extended to a representation of real and complex numbers in quantum mechanics. The work is based on the representation of real numbers as

equivalence classes of convergent Cauchy sequences of rational numbers. A representation of real numbers as convergent sequences of quantum states is being developed along with an equivalent operator representation.

<sup>1</sup>P. Benioff, Algorithmica **34**, 529-559, (2002).

<sup>2</sup>P. Benioff, Phys. Rev. A **63**, 032305 (2001).

## F. OTHER ACTIVITIES

### f.1. 16<sup>th</sup> Annual Midwest Theory Get-Together (C. D. Roberts)

The Theory Group hosted the sixteenth Annual Midwest Theory Get-Together on October 10-11, 2003. Nuclear theorists from six Midwest universities and ANL met to learn about the research goals and foci of different individuals and groups throughout the region. While the organizational duties rotate amongst the participants, Argonne is the regular host site because of its meeting facilities and central location. The organizer for 2003 was Charlotte Elster of Ohio University in Athens. The meeting provides a good chance for students to broaden their outlook and get some practical speaking experience in a friendly

atmosphere. The format is informal, with an agenda of talks being volunteered at the beginning of the meeting. In 2003 we had thirty-two registered participants: faculty, postdocs and students. Over the Friday afternoon and Saturday morning approximately twenty-five presentations were made, covering topics such as: relativistic heavy ion collisions; no-core shell model; nuclear pairing; nucleon matter; quantum Monte-Carlo methods; wavelet methods for few body physics; effective field theories; hadron physics; and QCD. No one left unwise.